Author:
Stankiewicz, Jan

Title:
Non-Linear Beam Bending of High Aspect Ratio Wing Aircraft

Non-Linear Beam Bending of High Aspect Ratio Wing Aircraft

By

Jan W. B. Stankiewicz BSc MInstP AMRAeS

Department of Aerospace Engineering
UNIVERSITY OF BRISTOL

A thesis submitted to the University of Bristol in accordance with the requirements of the degree of MASTER OF SCIENCE BY RESEARCH in the Faculty of Engineering.

SEPTEMBER 2018

Word count: 12,769

...to my Emma.

CONTENTS

ABSTRACT

Modelling and prediction of flutter and gust loads, and hence their suppression and alleviation, in high-aspect ratio wing (HARW) aircraft requires the study of highly-flexible wings that can undergo extremely large deflections. For modelling purposes and mathematical analysis, this thesis treats these highly-flexible wings as a flexible cantilever beam with a set bending and torsional rigidity. The use of simple linear methods can no longer be considered for the modelling of large deflections of cantilever beams, due to inaccuracies in curvature and geometric shortening effects of the deflected beams. A new method for the improvement of modelling large bending deflections of cantilever beams is proposed. The presented method accurately determines the 'actual bent' length of a cantilever beam undergoing a large deflection, possibly due to flutter excitation, turbulence or gust load. This calculated length is in concurrence with literature and unpublished literary findings and will hopefully aid in further, more complex flight flutter calculations, flutter prediction and gust load prediction models.

ACKNOWLEDGEMENTS

I would like to start by thanking Defence Equipment and Support (DE&S) of the Ministry of Defence for funding this degree. Thanking my line managers, graduate training managers, the Defence Engineering and Science Group (DESG) graduate office, mentors and technical development partners for the support given to me throughout this year.

I would like to thank all the PhD students, research associates and both technical and academic staff within the faculty of engineering for putting up with all my questions and dedicating their precious time to help me with issues and problems encountered throughout this degree. A special mention to my supervisors, Professor Jonathan Cooper, Dr. Dorian Jones and Dr. Robert Cook; all to whom I have eternal gratitude for the immense support and guidance throughout this year. I'd like to thank them for helping me with the academic work, especially as I did not major in aerospace engineering at undergraduate level.

Special thanks go to my family and friends for the support they provided me with during this year and for offering invaluable advice during tough times. It has been their encouragement and support that fuelled me with the motivation that enabled me to persevere and complete this degree.

Thank you all.

AUTHOR'S DECLARATION

I declare that the work in this dissertation was carried out in accordance with the Regulations of the University of Bristol. The work is original, except where indicated by special reference in the text, and no part of this thesis has been submitted for any other academic award. Any views expressed in the thesis are those of the author.

Signed: *J W B Stankiewicz* **Date:** *28/09/2018*

NOMENCLATURE

c	Chord
E	Elastic Modulus
I	Moment of Inertia
L	Length
L'	Shortened Length
P	Point Load
q	Generalised Co-ordinate Vector
Q	Generalised Force Term
s	True Arc Length
T	Kinetic Energy
t	Time
U	Elastic Potential Energy
W	Work Done
$\psi(z)$	Function of z
ζ	Dissipative Function for Non-Conservative Systems

ABBREVIATIONS

BM	Bending Mode
CoM	Centre of Mass
CAA	Civil Aviation Authority
COTS	Commercial Off The Shelf
CFD	Computational Fluid Dynamics
DE&S	Defence Equipment and Support
DoF	Degree of Freedom
EBT	Elementary Beam Theory
ETB	Engineering Theory of Bending
EAS	Equivalent Air Speed
FAA	Federal Aviation Administration
FE	Finite Element
FEM	Finite Element Method
FFT	Flight Flutter Test
FBD	Free Body Diagram
GVT	Ground Vibration Test
GLA	Gust Load Alleviation
HAR	High Aspect Ratio
LE	Leading Edge
LHS	Left Hand Side
LCO	Limit Cycle Oscillation
MOD	Ministry of Defence
NACA	National Advisory Committee for Aeronautics
NASA	National Aeronautics and Space Administration
RHS	Right Hand Side
RSJ	Rolled Steel Joist
TE	Trailing Edge
UAV	Unmanned Air Vehicle

LIST OF FIGURES

CHAPTER 1

1.1 Introduction

This thesis presents research into the modelling of high aspect ratio wings (HARW) undergoing large deflections. It examines research being conducted in several specialist fields of aeroelastics and covers relevant background information required to comprehend the path of research. The historical development of flutter and gust load prediction in aircraft is described and background information on the suppression of these two phenomena during flight is covered. Furthermore, it examines current research being conducted in the field of aeroelastics to model flutter and gust responses in aircraft using both linear and non-linear geometrically exact deflection methods, identifying potential gaps in current academic research conducted in this field.

A new method is then presented which corrects modelling inaccuracies that occur when aircraft wings undergo extremely large deflections as a result of static bending tests or mid-flight aeroelastic phenomena such as gust induced oscillations or flutter. This new method and research conducted mainly focuses on improving the modelling of flutter, flutter suppression, gust load modelling and gust load alleviation of high-aspect ratio wings. The research considers a HARW and highly flexible cantilever beam to represent a highly flexible aircraft wing.

1.2 Objectives of Research

The aim of the research conducted by the author in this thesis is to explore a new method of estimating the apparent shortening of a cantilever beam undergoing large deflections. There is

little current research that focuses on this shortening effect and traditional industrial approaches do not consider this effect.

Due to the inherent danger that is posed if flutter were to occur during flight, aircraft manufacturers prioritise the study of flutter amongst other aeroelastic and aerodynamic phenomena. Several modelling techniques are employed by aircraft manufacturers in conjunction with universities, with novel research being of paramount importance in suggesting better and improved ways of modelling and predicting the phenomena. The objectives of this research aim to:

- Aid the formulation of large bending of a long, uniform and static cantilever beam.
- Aid the formulation of large bending of a dynamic, long and uniform cantilever beam.
- Enhance current methodologies in the analysis and formulation of large bending of long, uniform cantilever beams and their application in aircraft and thus aiding and flutter and gust modelling techniques.

1.3 Structure of Thesis

This preliminary chapter of the thesis introduces the reader to the topic and describes the reasons for investigating non-linear beam bending in the suppression of flutter and alleviation of gusts in high aspect ratio wings.

Chapter 2 focuses on different aspects of aeroelastics. Each topic within this chapter contains a brief explanation on the topic area and literature review of research in this area; examples include ‘Flutter in Aircraft Wings’ and ‘Structural Modelling of Aircraft Wings and the Modelling of Flutter’. The following two chapters, Chapter 2 and 3, focus on the theory prerequisites required to comprehend the author’s research present in Chapter 4. Chapter 5 details the conclusions drawn from the research performed and Chapter 6 summarises any possible future work that could follow on from this work.

CHAPTER 2

HISTORY AND LITERATURE REVIEW

2.1 The History of Flutter

Ever since the development of the first aircraft, aircraft design has focused on minimising mass, achieving maximum lift with minimal drag and increasing fuel economy. This in turn has led to thinner, calibrated aerofoil shapes and through the use of composite materials, stronger and more stress-resistant aircraft wings have been developed. However, these alterations and with the addition of horizontal and vertical stabilisers, elevators, ailerons, spoilers and T-shaped tail configurations have resulted in an increase in the likelihood of non-linear aeroelastic effects and flutter, occurring within the flight envelope [1,2].

Prevention of flutter has been an urgent item on industry's agenda ever since the phenomenon was first encountered in December of 1903, by Professor Samuel Langley and his aerodrome, and by Orville and Wilbur Wright in the manufacture of their 1903 Flyer.

The Wright brothers successfully flew their biplane utilising aeroelastic effects to assist in aircraft control. They designed the biplane in such a way that the wings were warped, replacing the role of ailerons in providing control in the longitudinal or roll axis, as well as assisting in altering the longitudinal angle of flight and banking the aircraft. Orville and Wilbur [2,3] also encountered problems with a decline in thrust under high loads. The cause for this loss of thrust in the propellers was attributed to the abnormal aeroelastic effects that occurred when the

propellers reached high rotations per minute, undergoing an increase in load across the propeller tip. The aeroelastic effects caused tension at the leading edge of the blade and compression at the trailing edge of the blade, resulting in a slight buckling of the propeller. To account for this anomaly, triangular surface panels or "little jokers" were fitted to the trailing edge of the propeller blades to balance out the pressure causing the twisting of the blades. Following the success and increase in thrust at high speeds, the two brothers opted to remove these surfaces and instead decided to curve the trailing edges of the blades to give them a 'pre-bent' shape, giving them the name they were later known as [3].

Langley [2] experienced two structural failures when attempting to fly to his aircraft. The first, occurred through a launch mechanism failure, however the cause of the second failure is somewhat more complex. It involved the collapse of the rear tail and wing and although its exact cause is unknown, there have been several speculations by academics in the field of aeroelastics. Hill [4] proposed the cause of the failure could have been linked to insufficient wing-tip stiffness, thus producing wing torsional divergence, a catastrophic aeroelastic failure resulting in what essentially is flutter. In 1913, Brewer [5] suggested that the rear wing flip could have been caused by the length of the wing and its span, stating that "the greater the span the more readily will the wing tips be twisted". There seems to be a large amount of controversy surrounding Langley's machine and whether the aircraft was indeed capable of getting airborne prior to the Wright brothers if it weren't hindered by torsional divergence.

The first major progress in the identification of flutter was by Lanchester during the first world war. The Handley Page 0/400 biplane bomber suffered powerful oscillations of the main body and rear of the aircraft. Post-flight analysis conducted by Lanchester was performed to ascertain the cause of the almost-destructive vibrations. The aircraft's two elevators were

independently connected to the yoke; coupling of resonant frequencies from the two was therefore discarded as the possible cause of the condition and an alternative solution was devised. He suggested that the vibrations produced from their origin were self-excited. A similar lethal tail flutter incident was observed on a de Havilland DH.9 biplane bomber. Both of these issues were resolved through the implementation of a torsionally stiff tube to connect symmetrical elevators [2].

The first theoretical analysis of the condition was performed by Leonard Bairstow when performing supplementary analysis in Lanchester's investigations. Bairstow and fellow co-author Fage, published a paper [6] detailing the theory of the phenomenon. The paper focused on binary flutter of the system, consisting of two degrees of freedom. One degree of freedom around the longitudinal axis, or rigid body roll, and one degree of freedom around the lateral axis, predominantly the deflection of the aircraft's elevators. Bairstow's previous papers and mathematical formulations formed the foundations in establishing the equations of motion and characteristic equations governing the cause of the phenomenon. He describes quasistationary constants using aerodynamic derivatives, allowing for the solution to the quartic equations to be obtained, thus giving the corresponding eigenmodes and eigenvalues. This, combined with Routh's criterion allowed for detailed flutter analysis of the problem, and the determination of any aeroelastic instabilities, such as divergence. Bairstow's flutter analysis confirmed Lanchester's evaluation, providing a firm ground for flutter research in decades to come [2]. Furthermore, two years after Bairstow and Fage's [6] progress in the field of unstable aeroelastic and aerodynamic phenomena, Blasius [7] made several calculations following the collapse of the lower wing of the Albatross D.III biplane [8].

Although detailed estimates and analysis of the instabilities occurring in aircraft in the early 20th century were starting to emerge, definitive numerical calculations of the problems were not postulated until the 1920s. The reason for which, was the constricting and limited knowledge available on nonstationary aerofoil theory. The underlying theory was first construed in 1902, when Kutta published his work on irrotational flow around a circular arc. His paper, combined with Jowkowski's work in 1906 [59], resulted in the formulation of one of the more fundamental aerodynamic theorems to date.

Work on the field of unsteady aerodynamics was published in 1923 by Birnbaum [9], detailing vortex theory of the 2-D steady flow around thin aerofoils. He succeeded in developing his methodology to encompass a harmonically oscillating aerofoil in uniform flow. Birnbaum used concepts of vorticity distribution and Kelvin's theorem, expressing free vorticity as bound vorticity, to yield an integral expression for the pressure distribution in terms of perpendicular velocity at the aerofoil surface. A non-dimensional reduced-frequency was later introduced to produce an expansion series for the pressure distribution. Unfortunately, Birnbaum suffered from convergence difficulties, limiting the values for the reduced frequency and thus only being able to obtain numerical results up to a reduced frequency of 0.1 [2,8]. Further analysis on the harmonic effects was detailed by Wagner in 1925 [10], describing the growth of lift with respect to time, known in aerodynamics as the Wagner's function.

Significant progress was made in 1929 by Glauert [11], who following the aforementioned methodology by Wagner and other significant academics, was able to analyse a harmonically oscillating aerofoil and obtain a more successful result. Glauert derived integral expressions for the moment and lift and unlike Birnbaum, were not subject to complications in convergence. His analysis highlighted the issue of the possibility of low frequency flutter

occurring due to the negation of the damping moment in the equations during pitching. Glauert published a value of 0.5 for the reduced frequency [8].

In 1929, a paper on flutter by Küssner [12] was published, applying knowledge from Birnbaum's calculations to improve the numerical calculations, yielding a value of up to 1.5 for the aerodynamic coefficients. Küssner was not only able to improve Birnbaum's values, but eliminate the need for a time coordinate and introduce beam theory to replace the structure of a wing [8].

1934 marked the derivation of two-dimensional flutter, namely by Theodore Theodorsen. Theodorsen [13] published a paper, in which he stated that he has had success in determining "the aerodynamic forces on an oscillating airfoil or airfoil-aileron combination of three independent degree of freedom"; in essence, Theodorsen was able to produce an exact solution of a harmonically oscillating aerofoil, something the previously mentioned academic work failed to achieve due to the constraints of instability, equilibrium and convergence. He details that the solution, using potential flow and the Kutta condition is produced in the form of Bessel functions. Theodorsen was able to depict the velocity at which flutter occurs against the frequencies "in the separate degrees of freedom for any magnitudes and combinations of the airfoil-aileron parameters" [13]. Theodorsen work in the field of flutter in aeroelastics was recognised by Garrick, and was credited by him for a number of flutter-related studies [14].

The depiction of flutter analysis results was aided by Smilg and Wasserman [15], who in 1942, introduced a different type of flutter analysis procedure, known as the V-g method. This

method was used to graphically represent flutter solutions using the structural damping concept and the parameter *g* and the velocity [2,8].

It is obvious that the phenomenon of aeroelastic flutter was the cause of failure for a number of aircraft in the first half of the 20th century. It can also be noted that several destructive aircraft flight failures probably occurred due to incorrect mass distribution in different parts of the aircraft, such as ailerons [8]. Other accounts of research into flutter and aeroelastic instabilities in aircraft are present and undoubtedly significant in the field, however have not been further explored in this thesis.

Researchers in the past century have been able to identify the appearance of flutter in a non-aircraft-related setting. The cause of the collapse of the Tacoma Narrows bridge in the US state of Washington was originally attributed to externally forced resonance of the bridge under high winds [16,17]. A study published by Billah and Scanlan [18] in 1990 highlights the real reason for the failure of the bridge. The study details that wind passing across the structure produced vortices, which started the external forced excitation of the bridge. The structural damage that occurred at its point of failure was because of aerodynamically induced self-excitation in a torsional mode. The phenomenon that occurred in the Tacoma Narrows bridge case was complex separated-flow flutter in one torsional degree of freedom, as opposed to the coupling of bending and torsional modes found in aircraft wing flutter. Furthermore, the study seems to avoid the flutter term itself and promote the cause of failure being due to a "interactive aeroelastic phenomenon" between the wind and structure [18]. The author's reasoning focuses on the non-comparable difference in the two types of flutter; suggestions range from wind

velocity compared to the wind velocity in aircraft-type flutter, as well as the bridge structure and its aerodynamic fluid flow not meeting the Kutta condition.

It is therefore clear that flutter is indeed an extremely complex phenomenon in the field of aeroelastics, structural engineering and beyond.

2.2 Flutter in Aircraft Wings

2.2.1 A brief introduction into Flutter

The aeroelastic instability presents itself in multiple areas of engineering, not only in aircraft. The phenomenon of flutter can be described as the amalgamation of three different types of forces; aerodynamic, inertial and elastic forces, at specific critical conditions. These forces induce unstable oscillations within structures and in the majority of cases, result in catastrophic failure [1].

These unstable oscillations are often described as divergent oscillations that occur only above a certain speed, namely the flutter velocity, the point at which runaway occurs. The structure at this exact point undergoes simple harmonic motion (SHM) [50,51]. Oscillations that are induced below this velocity, are damped and do not cause any structural damage but could impact on performance of the structure. Whilst oscillations that are induced due to an internal or external disturbance, and occur at velocities higher than the flutter velocity threshold can lead to self-excited oscillations and structural failure of the structure, if not suppressed by any dampening systems or forces [53].

Flutter is difficult to predict and therefore where possible and when conditions can be foreseen, appropriate measures are taken to ensure the structure does not pass the flutter velocity threshold. If the structure is required to enter and surpass this threshold, suppression systems must be installed to actively suppress any occurrence of the aeroelastic phenomenon or it must be redesigned.

Traditional methods of preventing flutter, such as mass distribution, balancing and localised structural stiffening are often used. However, these methods are not the best methods as addition of mass to a structure may not necessarily favour the system, especially where weight is critical, such as in aircraft. Furthermore, these methods are not the only sole definitive solutions for the elimination of flutter [19].

2.2.2 Flutter in subsonic aircraft

As discussed, aeroelastic flutter is most commonly observed in aircraft, where aerodynamic surfaces and aircraft structures can suffer from dynamic instabilities and affect the fluid flow surrounding the structure, leading to potential positive feedback and the occurrence of unwarranted aeroelastic behaviour. In aircraft, as well as other aeroelastic systems, flutter can be categorised into two separate types, soft flutter and hard flutter. Soft flutter is defined as when the net damping gradually approaches critical flutter velocity and hard flutter is defined as when the damping values suddenly drop when approaching flutter velocity [54]. In aircraft, flutter occurs when the aircraft travels at the aforementioned critical speed or flutter velocity. Although this condition is true, both commercial and military aircraft are designed so that this flutter condition is not within the aircraft's design envelope. Complex aeroelasticity flutter analysis is carried out when designing aircraft parts, ensuring each part is free of flutter when in the flight envelope [1].

Aircraft components are intrinsically light and can experience large loads within the flight envelope. These components can deform and these deformations in turn disturb the fluid flow around the components to initiate the process of self-excitation [2]. Flutter in aircraft can arise due to many interactions, such as wing bending and torsion, wing torsion and control surfaces, wing and engine coupling and T-tail configuration. As well as in aeronautics, flutter can occur in Formula 1 vehicles, wind turbines, bridges and buildings to name a few.

Specialist mid-flight systems and pre-flight methods of analysis have been developed to tackle and eliminate the possibility of flutter occurring during aircraft flight. Ground vibration testing is carried out to collect vibration properties of the aircraft, such as natural frequencies of components, damping ratios and shapes of various modes. This information is then used in conjunction with theoretical flutter calculations to obtain more accurate flight flutter analysis [54].

Wind tunnel tests are also carried out on scaled models of the aircraft. These tests are used to determine pressure distributions, resultant forces and resultant moments at different speeds and different angles of attack. These factors allow for the determination of aerodynamic derivatives vital in aeroelastic and aerodynamic analysis. Wind tunnel flutter tests are also carried out to gather information that will aid computer models and any further aeroelastic analysis [54].

There are other tests that are carried out as per industrial practice and certification of the aircraft, however one of the most important tests that is carried out is the flight flutter test. This test is performed once the aircraft has passed all pre-flight tests and has been allocated a flight envelope. The aircraft is then taken for a test flight, with onboard measurement systems, recorders and accelerometers. A range of steps or test points are performed to push the aircraft

out of its current flight envelope and ascertain the aircraft's limit to vibration and flutter. This test is dangerous and therefore several test points are established and the results for extreme conditions are curve-fitted to avoid the aircraft leaving the envelope with potential of structural failure [54].

Recently, aircraft manufacturers are exploring installing active flutter suppression systems onboard the aircraft, which are linked to the onboard automatic control system. This system automatically activates and suppresses flutter through appropriate adjustments of the aircraft's control surfaces. There are several advanced control theories that govern the flutter suppression system, such as adaptive control, time delays and others. These are used in conjunction with sensors, digital controllers, filters and hydraulic actuators to effectively and instantaneously identify flutter and account for it. Currently, regulatory bodies prohibit aircraft to fly with flutter suppression systems. Relevant certification procedures, such as flight flutter tests are in place to ensure the flutter speed is not exceeded during flight [19-21,55].

2.2.3 Flutter in Aircraft with High-Aspect-Ratio Wings (HARW)

Flutter becomes important when considering aircraft with very high-aspect-ratio wings (HARWs).

Fig 1. Schleicher ASH glider with high-aspect-ratio wings. This aircraft has wings with an aspect ratio of 33.5 [48].

Although aircraft with HARW such as gliders have been around for a long time, novel high-aspect-ratio wing aircraft have only recently been fully exploited and the results have been extremely positive, with these aircraft achieving much higher performance than standard aspect ratio wing aircraft. HARW have a much higher lift-to-drag ratio, thus increasing its flight endurance, making them inherently more fuel efficient and appropriate for longer flights with increased range, suitable for a range of different commercial, government and military applications [52,56].

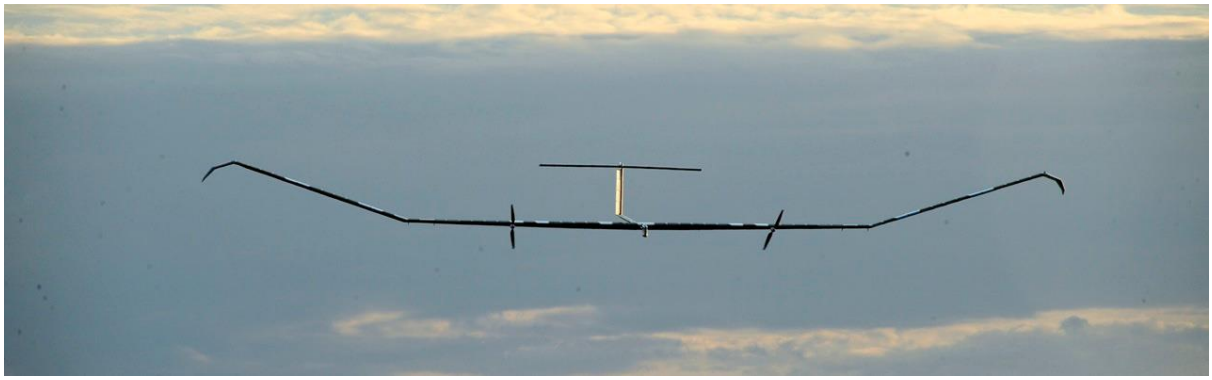

Fig 2. Zephyr 8 high altitude pseudo satellite (HAPS) with high aspect ratio wings [49].

High-aspect-ratio wings are often known as highly flexible wings, due to their large wingspan. Highly flexible wings have been essential in the field of unmanned air vehicles and high-altitude and long-endurance aircraft [24]. These aircraft can undergo extremely large wing deflections during flight. Furthermore, the flexibility also impacts the aircraft's performance. To fly at very high altitudes and low velocity, the aircraft's wings must be set to high angles of attack throughout its flight. Combining all these separate aeroelastic and aerodynamic conditions results in an aeroelastic system that is challenging to model and analyse. Applying standard linear aeroelastic analysis to model flight mechanics will not produce accurate results. Non-linear techniques to model aerodynamic and aeroelastic effects have to be employed [47].

The aforementioned conditions renders the aeroelastic phenomenon of flutter inherently challenging to model and predict in highly flexible wing aircraft. The phenomenon of flutter is based about linear progression, where tiny perturbations result in self-excited, exponential behaviour. Therefore calculating flutter speed, for example for a nonlinear system such as the high-aspect-ratio wing configuration in aircraft discussed above, would require the "linearization of a nonlinear model about a zero steady state" or "linearization of a nonlinear model about a nonzero steady state (nonlinear static equilibrium state)" [57]. Eigenvalue

analysis is then performed to calculate the flutter speed. It can be seen that the complexity of aeroelastic analysis increases and simple flutter speed calculations become challenging. Modelling of aeroelastic phenomena in nonlinear systems, such as HARW aircraft, will be discussed in the next chapter [57].

2.3 Structural Modelling of Aircraft Wings and the Modelling of Flutter

2.3.1 Linear Modelling

The modelling approach of an aircraft wing is dependent on wing design and flight condition. One can assume that a wing considered in this scenario, is a normal aircraft wing, with either a low or high aspect ratio and of simple rectangular shape. The wings can be modelled structurally as a simple cantilever beam.

The use of cantilever beams extends across several areas of engineering, ranging from actuators and energy harvesters in smart materials to cantilever transducers in atomic force microscopy [25-27]. Cantilever beams are also encountered in everyday life, such as rolled steel joists (RSJs) in the construction industry and of course, in the aerospace industry.

The Euler-Bernoulli beam theory is applied to model infinitesimal strains and small deflections in beams, and cannot be applied to model the large deflections that occur in highly flexible aircraft wings. This elementary beam theory model developed by Euler and Bernoulli therefore limits any aeroelastic analysis being performed on aircraft with high-aspect ratio wings. The large deflections are said to convert the system into a geometrically non-linear system, where non-linear analytical techniques have to be considered and applied in order to accurately perform aeroelastic and aerodynamic calculations.

2.3.2 Non-Linear Modelling

Modelling of aircraft with nonlinear wing configurations, such as high-aspect-ratio wing aircraft or abnormally curved or shaped wings therefore requires appropriate nonlinear modelling methods and techniques.

2.3.2.1 Non-Linear Bending and Cantilever Beams

A cantilever beam can be used to model a multi-dimensional version of the aircraft wing, using the cantilever beam as a direct model for the wing.

Modelling an aircraft wing using the aforementioned cantilever beam system requires several assumptions to be made which will be detailed throughout this report. A specific focus has been placed on modelling deflections for high aspect ratio wings, and therefore the cantilever beam considered in this research will no longer be subject to small deflections, but to large deflections. Modelling of non-linear beams invalidates the use of elementary beam theory (EBT) to obtain solutions for the problem, since this theory does not consider the square of the first derivative in curvature and does not correct for the apparent shortening in length of the beam when the beam is subject to a load [28]. Many studies looking at potential large deflections of beams assume no apparent change in length of the bent beam, which is incorrect.

A range of approaches to tackle the modelling of deflections have been taken over the past years, however, there has been an increasing number of studies on the modelling of large deflections and the inherent non-linear complexity associated with them. Although an approximation of the solution was obtained by Gross and Lehr in 1938 [29], Barten [30]

describes a method in which he calculates the deflection of a cantilever beam accounting for the aforementioned issues with the square of the first derivative. Barten considers the bending moment at specified coordinates under a load. Through integrals, boundary conditions and first and second incomplete and complete elliptic integrals, the deflection angle at a specific length is derived. Barten also continues to compare his work to Gross and Lehr's approximation by solving for maximum bending stress and length of the beam. It must be noted that he acquired his elliptic integral notation from Jahnke and Emde [31], in a study by them in 1943.

Bisshopp and Drucker [28] also derive the horizontal displacement, or the previously referred to 'apparent length in shortening' of the long cantilever beam, through the use of elliptic integrals. They develop an exact expression for the curvature of the beam through the use of the length of arc and the gradient angle, establishing the bending moment of the beam. By considering the beam to be inextensible they then use elliptic integrals to solve for the deflection and ultimately deflection per unit length and therefore the horizontal displacement of the cantilever beam. Barten's and Bisshopp and Drucker's solutions are the two main and largely referenced papers that involve the use of elliptic integrals.

A further study by Mattiasson also uses elliptic integrals to obtain numerical solutions of large deflections of cantilever beams. Although the study differs in that Mattiasson looks at determining methods for finite element analysis for geometrically nonlinear beams and frames and employs the use of elliptic integrals and the results from Barten and Bisshop and Drucker to do so. Other studies have also tackled large deflection problems using elliptic integrals. These studies include Timoshenko and Gere, 1961, Lau, 1964, Wang, 1997, Coffin and Bloom, 1999 and a remaining few [32].

A study that looks at small and large deflections of a cantilever beam, is a study conducted by Belendez et al. [33]. He considers the derivative of the Bernoulli-Euler relationship to derive the horizontal and vertical displacements at the tip of the beam, as well as deflection ratios and results in terms of various parameters. Belendez's approach focuses on converting non-linear differential equations of the beam deflection into an integral format and then integrating for the arc length and total length of the beam about a set angle. His findings then detail numerical results and their comparison to theoretical results.

Numerical integration techniques have proven to be one of the most popular choices in the field of aeroelastics. Iterative shooting techniques in particular, have been employed by several academics in the field, namely Freeman [34]; Wang and Watson [35]; Mau [36]; Lee and Oh [37]; and others.

Chen [38] published a study suggesting an integral approach to solve equations governing large deflections of cantilever beams. Chen uses a newly developed approach to solve the problem, basing his derivation on the research of Ang et al. [39]. He uses the bending moment-beam deformation relationship into trigonometry; and through the application of boundary conditions obtains the derivative of the arc length with respect to distance *y* and hence the inverse gradient for his model. It is interesting, that similarly to the approach detailed in Chapter 4, Chen accounts for the 'apparent shortening' of the beam upon large deformation. Chen analyses three scenarios, large deformation of a cantilever beam for a concentrated load, distributed load and a combined load. For concentrated loads, Chen's results are identical to Bisshop and Drucker's elliptic integral method. His approach has proven invaluable for the establishment of ideas for the author's work and his methods of convergence to establish the 'apparent shortened' length of the largely deflected cantilever beam were considered.

Different approaches to obtain solutions for problems with large deflections also exist. Finite Element (FE) analysis can be used in conjunction with iterative techniques, such as the Newton-Raphson method [32]. In his paper on finite element solutions, Golley [40] analyses the discrete elements of a piece of bent elastic with set flexural rigidity. He uses Hermite interpolation polynomials and Gauss quadrature to establish the bending moments and shape of the piece of elastic. Furthermore, Golley highlights the popularity of the Newton-Raphson method in the analysis of large deflections of cantilever beams using finite element analysis. Other academics in the field have also pursued similar routes, namely Schmidt [41] and Kooi [42].

A final approach into the investigation of large deflections, is the "incremental finite differences method in connection with Newton-Rhapson iteration techniques" [32]. Few studies exist that employ the use of this method, such as Kooi and Kuipers [43] and Safe and Srpcic [44]. The predominant reason for this, stems from the issue in the method causing divergence in large deflection and requires extremely lengthy computation times.

2.3.2.1 Non-Linear Modelling Techniques for Aeroelastic Phenomena in Low and High-Aspect-Ratio Wing Aircraft

Theoretical development for the modelling of aeroelastic behaviour has taken a plethora of shapes and forms within the past two centuries. Several different non-linear modelling techniques have been proven and established within the field of non-linear mechanics. Several academic papers have been published, detailing individual complex methodologies for creating accurate models for nonlinear structures in engineering.

The modelling of aeroelastic instabilities can facilitated through the use of simplified models. A aircraft wing can be modelled through computational modelling, such as finite element analysis. These methods allow for full three dimensional analysis, structural testing and aerodynamic testing through the use of programs such as MSC NASTRAN. Although relevant, these methods proved too time consuming for the given time limit and were not considered in this report; a more elementary approach was used.

Methods that have been used in literature to model aeroelastic effects in highly flexible aircraft are inherently extremely complex. Howcroft et al. [46] uses the Euler Ritz method against an Euler reference frame to statically model a Patil-Hodges highly flexible wing. The study utilises an array of shape functions, such as polynomial, reverse polynomial, Chebyshev and Legendre against set load cases.

In a further paper, Howcroft et al [46] in conjunction with Airbus UK details several different complex methods for the modelling of high-aspect ratio wings. The report utilises Patil et al.

[47] and his clamped high-aspect ratio half-wing, using a set of defined parameters as a base to compare each method. As previously mentioned in section 2.3.2.1, the first method detailed by Howcroft is a nonlinear iterative method using MSC NASTRAN. It does this by computing aerodynamic loads using the doublet lattice method for each separate defined lift surface. The program then analyses the results, combines them and is able to plot the deformed shape of the HARW wing. Howcroft highlights that this method relies on structures that behave linearly and therefore has limitations when considering larger scale non-linear structures [46].

The second method highlighted in Howcroft et al's report, is the NeoCASS or Next generation Conceptual Aero-Structural Sizing Suite. This complex analysis software focuses on a finite-volume approach utilising specific distanced nodes to establish a finite equilibrium equation of the bent wing. A subprogram within NeoCASS is then used to perform static nonlinear aeroelastic analysis similar to that of the previous method.

The third method detailed in the report is the intrinsic beam model. It uses beam definitions and reference frames to establish an intrinsic beam equation and then uses a finite-element (FE) method and spatial integration of strains and curvatures to compute beam equations used for aeroelastic analysis. The fourth method, relies on a reduced order model based on a continuous shape function and "is based around the expression of the wing deflection as a weighted sum of shape profiles" [46]. This method highlights the difficulty to model significant geometric non-linearities, such as very large deflections and hence the difficulty to account for "'tip-shortening'-type effects". The method does however account for this and alleviate the issue through a model reduction strategy which incorporated a local reference frame to keep the wing in a original frame whilst it deflects [46].

All of these methods, although very complex, delve deep into the modelling of high-aspect ratio wing aircraft, allowing for more accurate analysis and prediction, and therefore prevention of these aeroelastic phenomena.

2.3.2.2 Non-Linear Modelling Techniques for the Flutter Suppression and Gust Alleviation in Low and High Aspect-Ratio Wing Aircraft

Flutter suppression of high aspect ratio wings has played a fundamental part in preventing catastrophic incidents. Although methods such as traditional addition of mass, mass distribution and fuselage stiffening are still employed in modern aircraft, automated systems such as 'active flutter suppression', introduced in the 1970s now ensure aircraft do not reach the point at which the aeroelastic instabilities occur. The phenomenon is supressed by the automated motion of control surfaces on each wing and tail [19]. The system itself utilises several different control theories, such as optimal control and adaptive control [20,21].

Gust alleviation in aircraft has also played a significant part in aviation history. The analysis of aircraft response to discrete and random gusts is paramount due to the condition's severity, which could result in destructive failure. High aspect ratio wing aircraft, such as unmanned aerials vehicles (UAVs) are especially susceptible to gusts, due to their long wing span and light structure. Large deformations can occur as a result of these gusts, which can lead to disturbance within the flight envelope, incurring possible subsequent non-linear aeroelastic instabilities [22].

Different modelling techniques have been employed over recent years to attempt to model aircraft wing gust response. The common method of gust response analysis has been through the use of the doublet-lattice method incorporated with the equations of motion for a flexible aircraft [23].

Su and Cesnick [24] employed the use of a “low-order nonlinear strain-based finite elemental framework” to analyse the nonlinear geometric effects of highly aspect ratio wings. They were able to model these discrete disturbances through the aforementioned framework and the incorporation of unsteady aerodynamics.

On the other hand, Dong et al. [23] detailed in his study the method for gust response analysis of flexible aircraft through the use of computational fluid and structure dynamics as well as computation flight mechanics. The method he employs utilises a computationally coupled flight and structural mechanics solving mechanism to depict free flight motion in the time domain. Further methods are then used to performed specialist aerodynamic, aeroelastic and structural calculations.

2.3.3 Summary

It is clear from literature that several approaches and methods have been used to tackle the large deflection of cantilever beams problem. The methods range from elliptic integral approaches, to numerical integration, to finite element analysis and finally incremental finite differences with the use of the Newton-Raphson iterative techniques. It is clear the author’s path of research focuses on a gap in literature, that has only recently been touched upon by Chen and his work on an integral approach [38].

CHAPTER 3

THEORY

3.1 Static Cantilever Beam Modelling – Equation of Motion

As a prerequisite for the introduction of the author's presented research, a short introduction on the Rayleigh-Ritz 'Assumed Shapes' method is discussed. The system that is considered is used to portray deformation of a beam, through a series of deformation shapes that are multiplied by an unknown, generalised coordinate. This method, using two bending modes is employed as a simple, light cantilever beam model, as seen in Chapter 4.

Consider an inextensible, simple, static cantilever beam of length L. This beam is fixed at the z-axis and is free to move in the z-y plane, under a specific vertical point load P applied at the tip of the beam. The flexural rigidity, EI, of the beam is constant, and non-varied through the beam. The theoretical setup is depicted in figure 3 below.

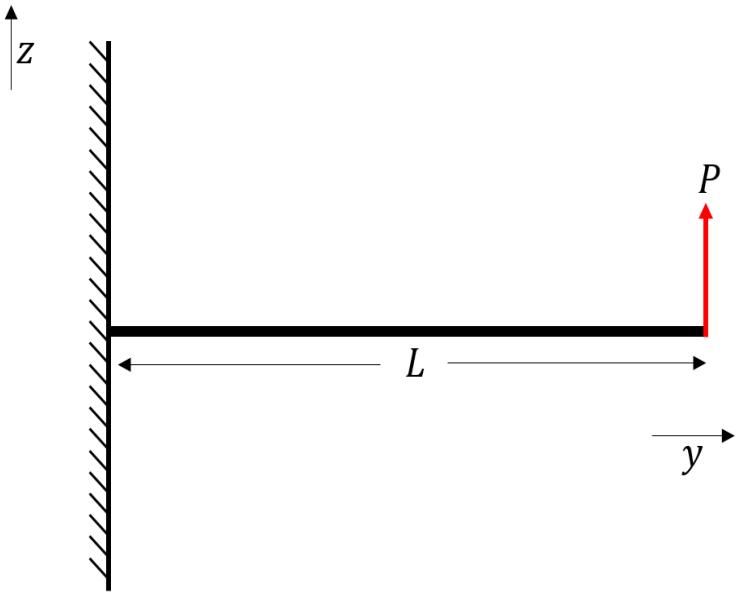

Fig 3. Static undeflected cantilever beam length L, just before bending occurs due to vertical point load P, applied at distance L, the tip of the beam.

The bending of this cantilever beam is approximated by considering a "set" deformation bending shape for the first two bending shape functions,

$$\psi_1(y) = y^2 \text{ and } \psi_2(y) = y^3 \tag{3.1}$$

within the function,

$$z(y,t) = \sum_{i=1}^{2} \psi_i(y) q_i(t) \tag{3.2}$$

to give,

$$z(y,t) = q_1(t)\, y^2 + q_2(t)\, y^3 \tag{3.3}$$

where *z* is the vertical bending displacement of the beam, *y* is the horizontal displacement of the beam, $q_1(t)$ is the first generalised coordinate of the system, and $q_2(t)$ is the second generalised coordinate of the system. From this point onwards, the notation of the generalised coordinates $q_i(t)$ $(i = 1..2)$, will be shortened to q_i $(i = 1..2)$, for clarity.

The generalised coordinates for the polynomial, shown in equation 3.3 can be determined through simple Lagrangian mechanics and static analysis of the above system. Initially, the elastic potential energy, U, of the system is determined. This strain energy is dependent on the second derivative of displacement and flexural rigidity and is given by

$$U = \frac{1}{2}\int_0^L EI\left(\frac{\partial^2 z}{\partial y^2}\right)^2 dy \tag{3.4}$$

$$\therefore U = \frac{1}{2}\int_0^L EI(\,2q_1 + 6q_2 y\,)^2\, dy \tag{3.5}$$

$$\therefore U = 2EI(q_1{}^2 L + 6q_1 q_2 L^2 + 6q_2{}^2 L^3). \tag{3.6}$$

Secondly, the work done by the point load at length $a = L$ is considered. The instantaneous work done term, δW, for this two-shape bending system is

$$\delta W(t) = P(t)\delta z(a,t) = P(t)[\delta q_1 L^2 + \delta q_2 L^3] \tag{3.7}$$

where $P(t)$ is the time dependant vertical point load. The incremental displacement of the system, $\delta z(a,t)$, is rewritten in terms of increments of the generalised coordinates, δq_i $(i = 1..2)$. The magnitude of the applied load at distance a from the origin is therefore dependant on the bending mode shape of the system.

The modified Lagrange's equation written in terms of generalised coordinates q_i $(i = 1..2)$, is now applied incorporating the above derived energy and work terms for the continuous system.

$$\frac{d}{dt}\left(\frac{\partial T}{\partial \dot{q}_i}\right) - \frac{\partial T}{\partial q_i} + \frac{\partial \zeta}{\partial \dot{q}_i} + \frac{\partial U}{\partial q_i} = Q_i = \frac{\partial(\delta W)}{\partial(\delta q_i)} \;\; where\; i = 1..2 \tag{3.8}$$

where U is the elastic potential energy, $\zeta$is the dissipative power for non-conservative systems, Q_i is the generalised force term and T is the kinetic energy. The notation $\dot{q}_i$ denotes the

derivative of q_i with respect to time. The system in figure 3 is a static scenario with no dissipative forces, therefore the kinetic energy and dissipative function in equation 3.8 is ignored.

To determine $\frac{\partial U}{\partial q_i}$, the elastic potential energy in equation 3.8 is differentiated with respect to each individual generalised coordinate separately, as shown below in equations 3.9 and 3.10.

$$\frac{\partial U}{\partial q_1} = EI[4q_1L + 6q_2L^2] \tag{3.9}$$

$$\frac{\partial U}{\partial q_2} = EI[6q_1L^2 + 12q_2L^3] \tag{3.10}$$

These two equations and the work term from equation 3.7, now yield two simultaneous equations of motion when processed using the aforementioned Lagrangian, shown below.

$$4EIq_1L + 6EIq_2L^2 = P(t)L^2 \tag{3.11}$$

$$6EIq_1L^2 + 12EIq_2L^3 = P(t)L^3 \tag{3.12}$$

The joint result, therefore, in matrix form becomes

$$EI\begin{bmatrix} 4L & 6L^2 \\ 6L^2 & 12L^3 \end{bmatrix}\begin{Bmatrix} q_1 \\ q_2 \end{Bmatrix} = P(t)\begin{Bmatrix} L^2 \\ L^3 \end{Bmatrix}. \tag{3.13}$$

This equation takes the form of a classical multiple degree of freedom system, with the

stiffness matrix on the LHS of the equation but with dampening and mass matrices omitted. Solving these equations, gives

$$q_1 = \frac{1}{2}, \qquad q_2 = -\frac{1}{6}. \tag{3.14}$$

(3.15)

Substituting these values into equation 3.3, gives us the complete normalised equation modelling the deflection at a point (z, y), also depicted in figure 4.

$$z(y,t) = \frac{1}{2}y^2 - \frac{1}{6}y^3. \tag{3.16}$$

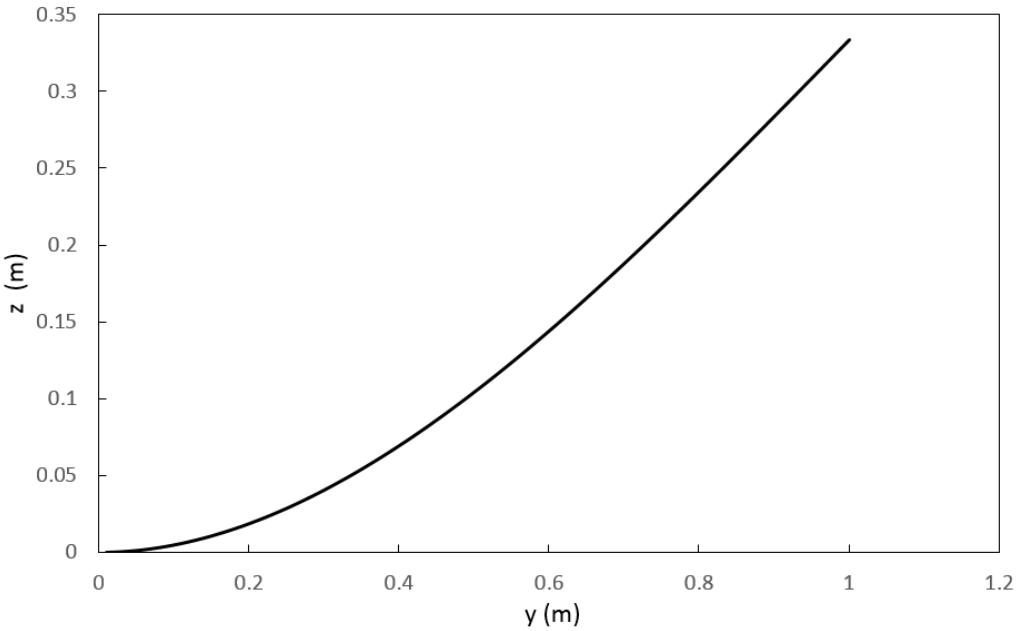

Fig 4. Depiction of the polynomial curve in equation 3.16, from y = 0 to 1.

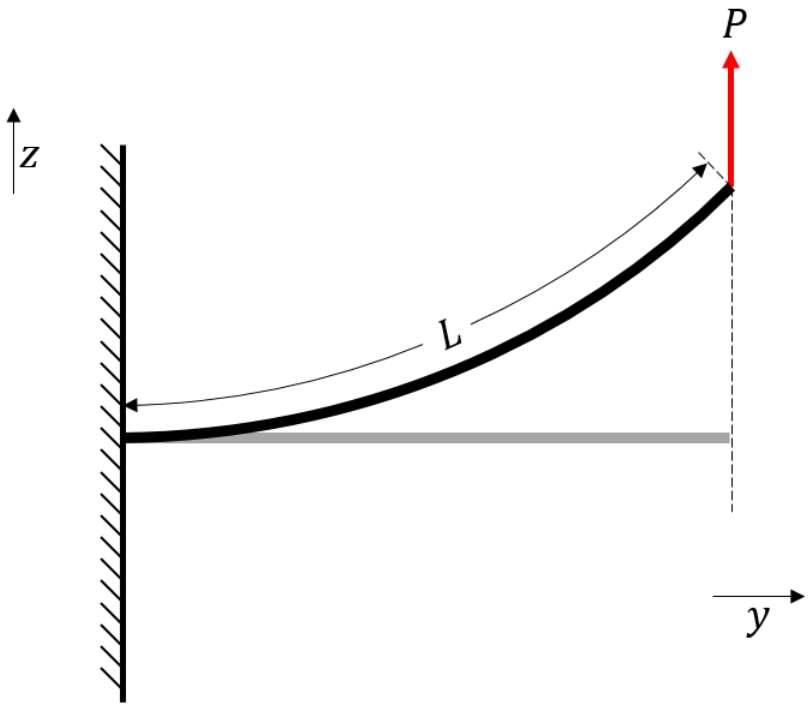

Fig 5. Physical representation of the polynomial model of cantilever beam (equation 3.16) after its initial deflection, due to the force P applied at length L. The grey bar illustrates the initial position of the cantilever beam (if considering a linear model), just before bending occurs.

The polynomial above now represents a model of the deflection of the cantilever beam from figure 3. Figure 5 illustrates the linearly calculated deflection of the cantilever beam and how figure 4 is a similar depiction of this deflection.

CHAPTER 4

RESEARCH

Unfortunately, the deflection in the z-y plane of the cantilever beam, based on the polynomial model in equation 3.16 and depicted in figures 4 and 5 is not a true representation of the actual bending of a cantilever beam. The cantilever beam ‘shortens’ in the horizontal plane. This system assumes the work done due to the point load at length L (figure 5) is the same as the work done post-deflection at distance L along the beam. This is incorrect, as the coordinates of the tip of the cantilever beam change upon deflection, modifying the distance the force is applied at, hence altering the work done.

This dilemma requires the apparent horizontal length of the deflected beam to be identified. To do this, the arc length of the polynomial as to be considered and a new method has to be devised to approximate the arc length of the deflected beam relative to its horizontal un-bent, initial-state length.

4.1 HARW Large Deflection Bending Correction Method

Figure 6 shows the correct scenario as described above, now accounting for an altered or 'shortened' horizontal displacement of the beam. The potential energy of the beam remains the same and the actual length of the beam, the original length L also remains the same.

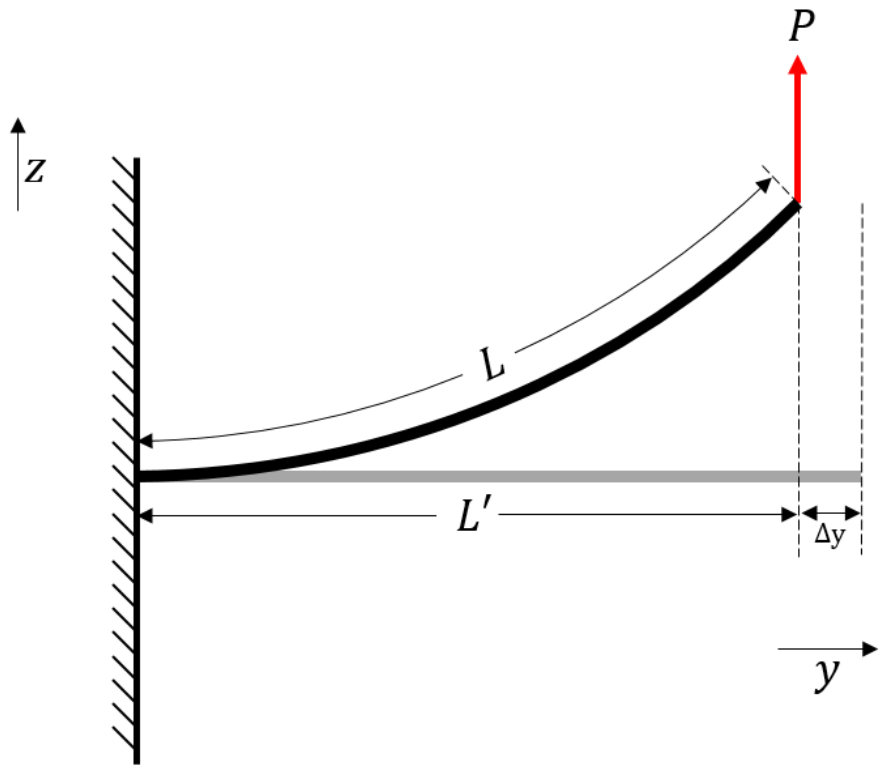

Fig 6. Modified physical representation of the polynomial model of cantilever beam after its initial deflection, due to the force P applied at length L. The grey bar illustrates the initial position of the cantilever beam, just before bending occurs. L′ is the 'shortened' horizontal displacement of the beam. Δy is the change in horizontal displacement of the beam during bending.

By inspection, the work done on the system, now acts at a different set of coordinates in the z-y plane. The coordinates become

$$\left(\left(\frac{1}{2}(L')^2 - \frac{1}{6}(L')^3\right), L'\right) \tag{4.1}$$

where L' is the 'shortened' horizontal displacement of the beam.

To calculate the 'shortened' horizontal displacement of the beam, a method of approximation has to be devised to find the coordinates of the altered position upon initial bending.

To do this, the length of the bent beam, or arc length, L, has to be considered. To calculate the arc length, the curve has to be approximated through individual discretised segments. Through the use of the mean value theorem, the approximation can be transformed into a derivative and subsequently, the sum of straight line segments can be converted into an integral. To perform this derivation, two assumptions have to be made. It is assumed the polynomial function in equation 4.2 is planar and that it is continuously differentiable over its entire considered length.

For ease of derivation, the principle will be applied to a planar curve with equation

$$z_j = f\ y_j. \tag{4.2}$$

The arc length will be calculated over a set interval between two points, depicted in figure 6; for the purposes of the derivation, this will be [A,B]. Initially, the interval is segmented into individual horinzontal components of length

$$A = y_0 < y_1 < y_2 < y_3 \ldots . < y_n = B. \tag{4.3}$$

Each segment distance is calculated as per the standard Euclidean metric and defined as

$$D_i = \sqrt{{\Delta y_j}^2 + {\Delta z_j}^2}\ , \quad \text{where} \quad \Delta y_j = y_j - y_{j-1},\ \Delta z_j = f y_j - f y_{j-1} = z_j - z_{j-1}. \tag{4.4}$$

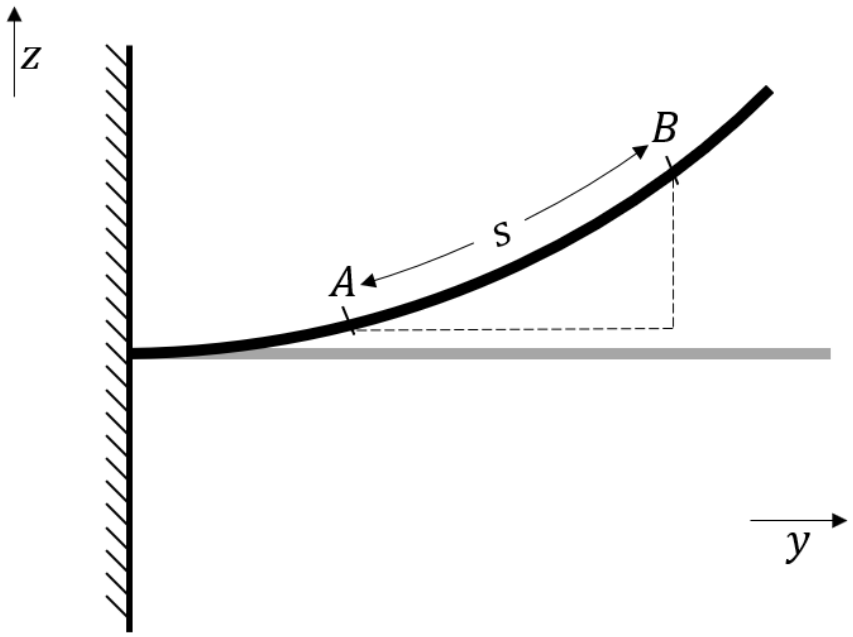

Fig 6.1. Points A and B along a curve setting boundaries for the interval used within this derivation. The true arc length, *s*, has also been depicted within the figure.

To obtain a value of the true arc length, s, in the interval [A,B] of the planar curve in equation 4.2, the limit to infinity of the distance of each segment has to be taken, shown below.

$$s \approx \sum_{j=1}^{N} D_j = \sum_{j=1}^{N} \left\{ \sqrt{{\Delta y_j}^2 + {\Delta z_j}^2} \right\} = \sum_{j=1}^{N} \left[\left\{ \sqrt{1 + \left(\frac{\Delta z_j}{\Delta y_j} \right)^2} \right\} \Delta y_j \right] \qquad (4.5)$$

Limit of N to infinity, gives

$$s = \lim_{N \to \infty} \sum_{j=1}^{N} \left[\left\{ \sqrt{1 + \left(\frac{\Delta z_j}{\Delta y_j} \right)^2} \right\} \Delta y_j \right] \qquad (4.6)$$

where N is the upper bound of summation, and, $j = 1$ is the index and lower bound of summation.

Applying the Mean Value Theorem,

$$f'\left(C_j\right) = \frac{fy_j - fy_{j-1}}{y_j - y_{j-1}} = \frac{z_j - z_{j-1}}{y_j - y_{j-1}} = \frac{\Delta z_j}{\Delta y_j} \tag{4.7}$$

where C_j is a point lying between $[y_j, y_{j-1}]$. The gradient of the segment in question can therefore be replaced with the derivative of the planar function.

$$s = \lim_{N\to\infty} \sum_{j=1}^{N} \left[\left\{\sqrt{1 + \left(f'\left(C_j\right)\right)^2}\right\} \Delta y_j\right] \tag{4.8}$$

Converting the summation into an integral, assuming a continuous function, gives

$$s = \int_{y_1}^{y_2} \sqrt{1 + \left(f'(y)\right)^2}\, dy \equiv \int_{y_1}^{y_2} \sqrt{1 + \left(\frac{dz}{dy}\right)^2}\, dy \tag{4.9}$$

the equation for the length of an arc [58]. This equation can now be taken and will form the basis in calculating the 'shortening' of the horizontal displacement of the beam.

To determine the y coordinate of the new location of the tip of the beam when initially deflected, the derivative of the modelling polynomial in equation 3.16 can be used in computing the arc length of the bent beam.

$$s = \int_0^{L'} \sqrt{1 + \left(\frac{dz}{dy}\right)^2}\, dy \quad \text{where} \quad \frac{dz}{dy} = y - \frac{1}{2}y^2. \tag{4.10}$$

To form this equation into a more solvable form, take equation 4.10 and let

$$\sqrt{1+\left(\frac{dz}{dy}\right)^2} \equiv \sqrt{1+(X)^2} \quad \text{where} \quad \frac{dz}{dy} = X \tag{4.10a}$$

Assume equation 4.10a is integrated with respect to X, as a generalised form of the equation.

$$\therefore \quad \int_0^{L'} \sqrt{1+(X)^2}\, dX \tag{4.10b}$$

Taking the integrand from equation 4.10b, substitute $X = \tan(u)$ and $dX = sec^2(u)du$, where u is a constant. This results in

$$\sqrt{1+(X)^2} \;= \sqrt{1+tan^2(u)} \;= \sec(u) \quad \text{and} \quad u = tan^{-1}(X) \tag{4.10c}$$

giving

$$\int sec^3(u)du \tag{4.10d}$$

Using the reduction formula,

$$\int sec^m(u)du = \frac{\sin(u)sec^{m-1}(u)}{m-1} + \frac{m-2}{m-1}\int sec^{-2+m}(u)du \tag{4.10e}$$

with the constant $m = 3$, gives

$$\frac{1}{2}\tan(u)\sec(u) + \frac{1}{2}\int sec(u)du \tag{4.10f}$$

Multiply the numerator and denominator of $\sec(u)$ by $\tan(u) + \sec(u)$, giving

$$\frac{1}{2}\tan(u)\sec(u) + \frac{1}{2}\int \frac{sec^2(u) + \tan(u)sec(u)}{\tan(u)+\sec(u)}du \tag{4.10g}$$

For the integrand on the RHS of equation 4.10g, substitute $w = \tan(u) + \sec(u)$ and $dw = sec^2(u) + \tan(u)\sec(u)\,du$, where *w* is a constant, giving

$$\frac{1}{2}\tan(u)\sec(u) + \frac{1}{2}\int \frac{1}{w}\,dw \tag{4.10h}$$

Integrating $1/w$ with respect to *w*, is $\log(w)$ and therefore gives

$$\frac{1}{2}\tan(u)\sec(u) + \frac{\log(w)}{2} + \mathrm{C} \tag{4.10i}$$

where *C* is a constant of integration. Substitute back for $w = \tan(u) + \sec(u)$ giving

$$\frac{1}{2}\tan(u)\sec(u) + \frac{1}{2}\log(\tan(u) + \sec(u)) + \mathrm{C} \tag{4.10j}$$

Substituting back for $u = tan^{-1}(X)$ gives

$$\frac{1}{2}\tan(tan^{-1}(X))\sec(tan^{-1}(X)) + \frac{1}{2}\log(\tan(tan^{-1}(X)) + \sec(tan^{-1}(X))) + \mathrm{C} \tag{4.10k}$$

This equation can now be simplified, with a constant z, by using $\sec\left(tan^{-1}(z)\right) = \sqrt{z^2 + 1}$ and $\tan\left(tan^{-1}(z)\right) = z$ giving

$$\frac{1}{2}\left(\sqrt{X^2 + 1}\right)X + \frac{1}{2}\log\left(\sqrt{X^2 + 1} + X\right) + \mathrm{C} \tag{4.10l}$$

and displaying the RHS in an alternate form, finally gives

$$\frac{1}{2}\left(\left(\sqrt{X^2 + 1}\right)X + sinh^{-1}(X)\right) + \mathrm{C} \tag{4.10m}$$

Substituting X back for $\frac{dz}{dy}$ from into the original equation 4.10 results in

$$s = \frac{1}{2}\int_0^{L'}\left[\left(\sqrt{\left(\frac{dz}{dy}\right)^2 + 1}\right)\left(\frac{dz}{dy}\right) + \left(\sinh^{-1}\left(\frac{dz}{dy}\right)\right)\right]dy\,. \tag{4.11}$$

The arc length, s, as shown in figure 6, is the original length of the cantilever beam, L. Substituting in to the above equation, gives

$$L = \frac{1}{2}\int_0^{L'}\left[\left(\sqrt{\left(\frac{dz}{dy}\right)^2 + 1}\right)\left(\frac{dz}{dy}\right) + \left(\sinh^{-1}\left(\frac{dz}{dy}\right)\right)\right]dy\,. \tag{4.12}$$

L', the 'shortened' horizontal deflection of the beam can therefore be solved for, providing L is known. However, integration and further analysis of equation 4.12 proves the solutions to be of an elliptic nature and hence the solution cannot be solved for symbolically.

To account for this issue, a mathematical approximation must be used to approximate $\sqrt{1 + \left(\frac{dz}{dy}\right)^2}$. To do this, a Taylor series approximation is used, to a set value of terms, expanding about a set value. The process is shown below.

$$\text{Let } \sqrt{1 + \left(\frac{dz}{dy}\right)^2} = \sqrt{1 + X^2} \quad \text{where} \quad X = \left(\frac{dz}{dy}\right) \tag{4.13}$$

The Taylor series is defined as,

$$f(X) = \sum_{n=0}^{\infty} \frac{f^{(n)}(a)}{n!}(X - a)^n \tag{4.14}$$

Applying equation 4.13 to equation 4.14, gives

$$f(X) = \frac{X^2}{2} + \frac{X^4}{8} - \frac{X^6}{16} + \frac{X^8}{128} \ \ldots \ \cong \sqrt{1 + X^2} \tag{4.15}$$

Equation 4.15 is now used in combination with equation 4.10, to give

$$L = \int_0^{L'} \left(\frac{X^2}{2} + \frac{X^4}{8} - \frac{X^6}{16} + \frac{X^8}{128} \ \ldots \right) dy \quad \text{where} \quad X = \frac{dz}{dy} = y - \frac{1}{2} y^2 \tag{4.16}$$

which when solved for, yields a value of L' depending on the length of the beam L. The mathematical code written in Matlab[a] to perform this calculation, produces a large range of solutions, many of which are too large, complex or imaginary. The code sifts through the data and filters out anomalous results, outputting the correct corresponding 'shortened' horizontal displacement.

Since the 'shortened' horizontal displacement has been calculated, the work done term in equation 3.7 can be reconsidered. The equations of motion for the **first deflection iteration** in matrix form from Chapter 3 are,

$$EI \begin{bmatrix} 4L & 6L^2 \\ 6L^2 & 12L^3 \end{bmatrix} \begin{Bmatrix} q_1 \\ q_2 \end{Bmatrix} = P(t) \begin{Bmatrix} L^2 \\ L^3 \end{Bmatrix} \tag{4.17}$$

[a] Matlab code available upon request.

However, following the first deflection, the coordinates at which the point load is applied to differ, at the aforementioned new horizontal displacement value L' along the y-axis. Therefore, the equation of motion for the **second deflection iteration**, with work done acting at $\left(\left(\frac{1}{2}(L')^2 - \frac{1}{6}(L')^3\right), L'\right)$ becomes

$$EI\begin{bmatrix} 4L & 6L^2 \\ 6L^2 & 12L^3 \end{bmatrix}\begin{Bmatrix} q_1' \\ q_2' \end{Bmatrix} = P(t)\begin{Bmatrix} L'^2 \\ L'^3 \end{Bmatrix} \tag{4.18}$$

and subsequently, the equation of motion for the **third deflection iteration**, with work done acting at $\left(\left(\frac{1}{2}(L'')^2 - \frac{1}{6}(L'')^3\right), L''\right)$ becomes

$$EI\begin{bmatrix} 4L & 6L^2 \\ 6L^2 & 12L^3 \end{bmatrix}\begin{Bmatrix} q_1'' \\ q_2'' \end{Bmatrix} = P(t)\begin{Bmatrix} L''^2 \\ L''^3 \end{Bmatrix} \tag{4.19}$$

and subsequent to that, the equation of motion for the **fourth deflection iteration**, with work done acting at $\left(\left(\frac{1}{2}(L''')^2 - \frac{1}{6}(L''')^3\right), L'''\right)$ becomes

$$EI\begin{bmatrix} 4L & 6L^2 \\ 6L^2 & 12L^3 \end{bmatrix}\begin{Bmatrix} q_1''' \\ q_2''' \end{Bmatrix} = P(t)\begin{Bmatrix} L'''^2 \\ L'''^3 \end{Bmatrix} \tag{4.20}$$

and so on and so forth, until the horizontal displacement increment converges into a fixed position – the final, correct y-value of the tip of position of the bent cantilever beam. It is important to note that a new set of generalised coordinates is generated each time to ensure the potential energy of the system remains the same. This process is depicted in figure 7.

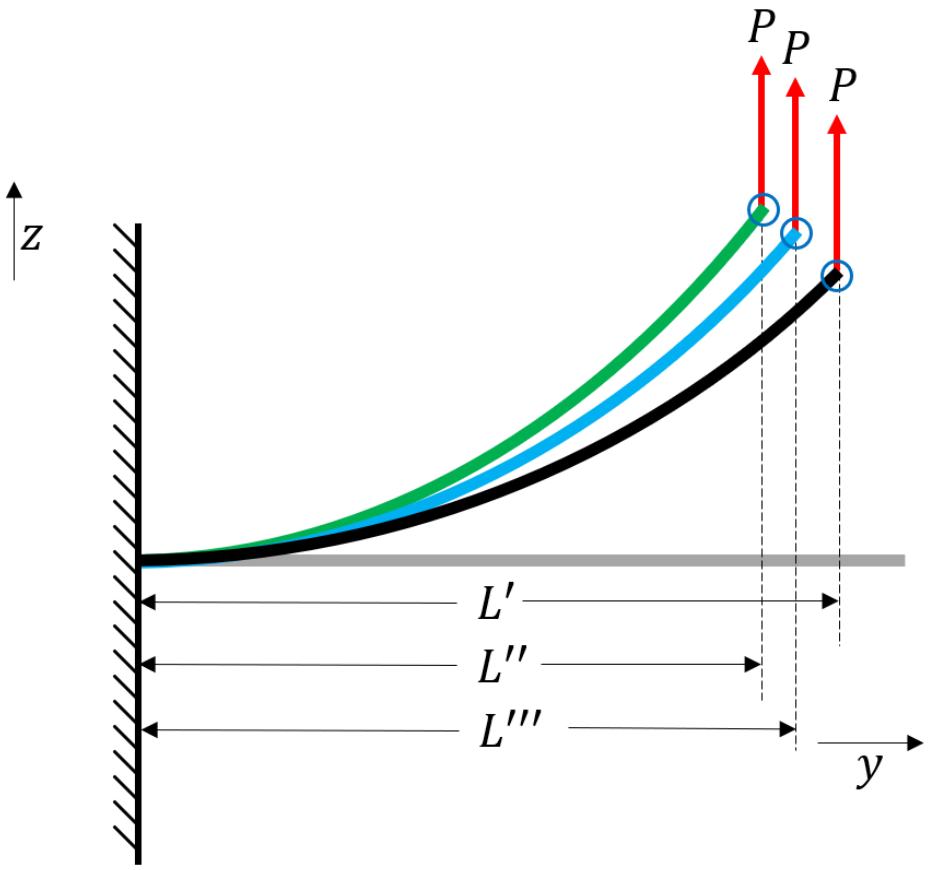

Fig 7. Modified physical representation of the polynomial model of cantilever beam after its initial deflection, due to the force P applied at length L. The grey bar illustrates the initial position of the cantilever beam, just before bending occurs. L′ is the 'shortened' horizontal displacement of the beam, obtained following the first deflection of the beam. L″ is the 'shortened' horizontal displacement of the beam, obtained following the second deflection of the beam. The changing coordinates of the work done during each deflection iteration is circled. The force P does not differ in magnitude or direction through all the deflections. By inspection, it can be seen that L″- L‴< L′- L″< L, therefore the 'shortened' horizontal displacement of the beam converges.

4.3 Static Cantilever Beam - Convergence Study

To compute an accurate graphical model of the deflection of the cantilever beam using the polynomial in equation 4.21 and the Taylor series in equation 4.15, the number of terms of the Taylor series and the number of deflection iterations must be considered and evaluated. In addition, the number of bending modes employed in the formulation of this equation is a major contributor to the accuracy of the bending model.

4.3.1 Taylor 'Number of Terms' Variation

Figure 8 and figure 8.1 show the variation in the computed value of the tip position (both z and y coordinates) for 20 deflection iterations of a cantilever beam with a L of 16m, varying the number of terms in the Taylor series. The point load applied is 200N and 150N respectively, for 2 bending modes; the polynomial equation of which, is

$$z(y,t) = q_1(t)\, y^2 + q_2(t)\, y^3 \tag{4.21}$$

as previously derived.

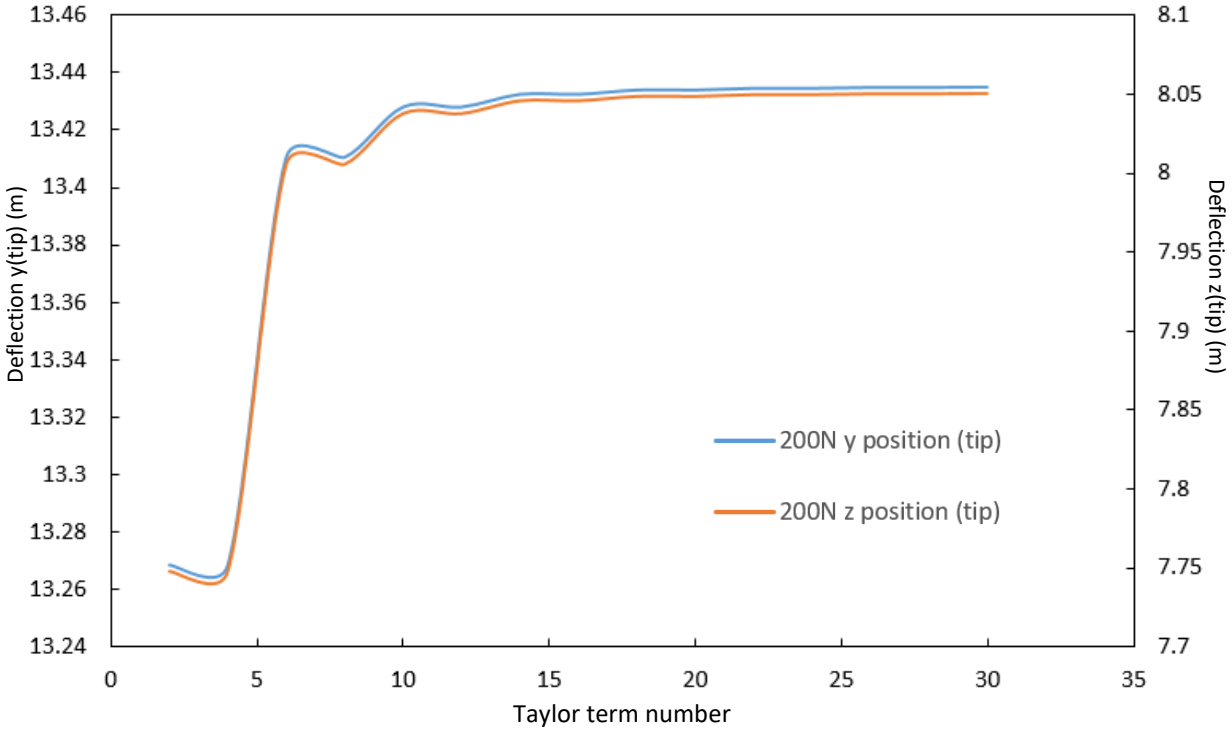

Fig 8. Convergence of the y and z coordinate of the beam tip position of a cantilever beam undergoing a deflection caused by a vertical tip load of 200N, following 20 deflection iterations for two bending modes. The number of terms in the Taylor series (y-axis) increases and the corresponding z-value (m) converges.

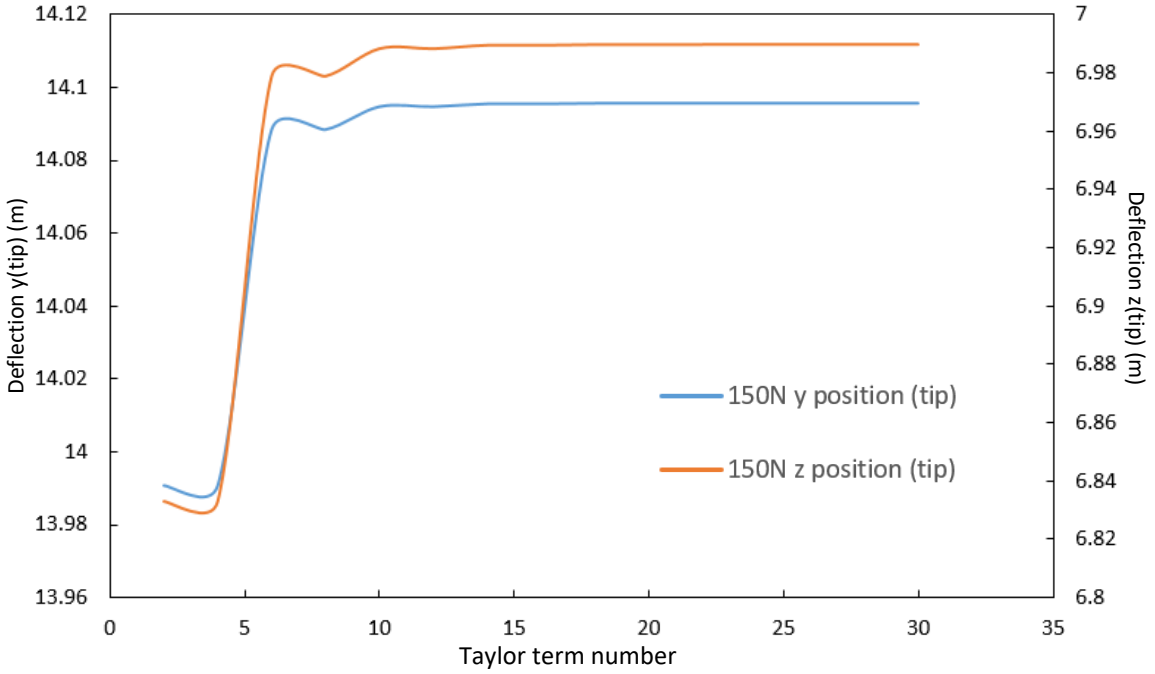

Fig 8.1. Convergence of the y and z coordinate of the beam tip position undergoing a deflection caused by a 150N vertical tip load for 2 bending modes, following 20 deflection iterations. The number of terms in the Taylor series (y-axis) increases and the corresponding z coordinate value (m) converges.

4.3.2 Deflection Iteration Variation

Similarly to the number of terms in the Taylor series, the number of deflection iterations is extremely important, depicted in figures 8.x in the previous section. The following set of figures show the effect of increase of deflection iterations for 150N and 200N tip point loads. Again, a two bending mode system is considered, as portrayed in equation 4.21.

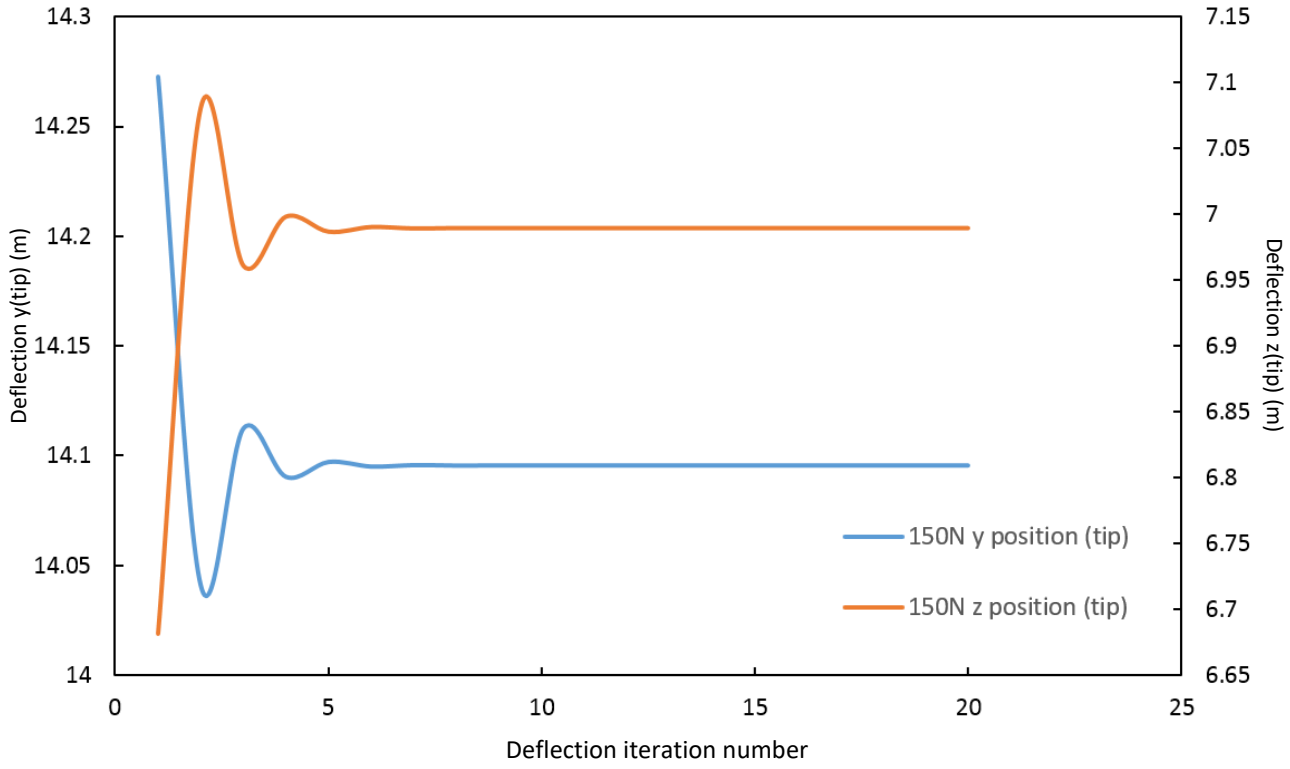

Fig 9. 150N Vertical Tip Load and 2 Bending Modes. Convergence of the y and z coordinate of the beam tip position, following 20 deflection iterations and using 30 number of terms in the Taylor approximation. As the number of deflection iterations increases, the z and y coordinate of the cantilever beam tip converge.

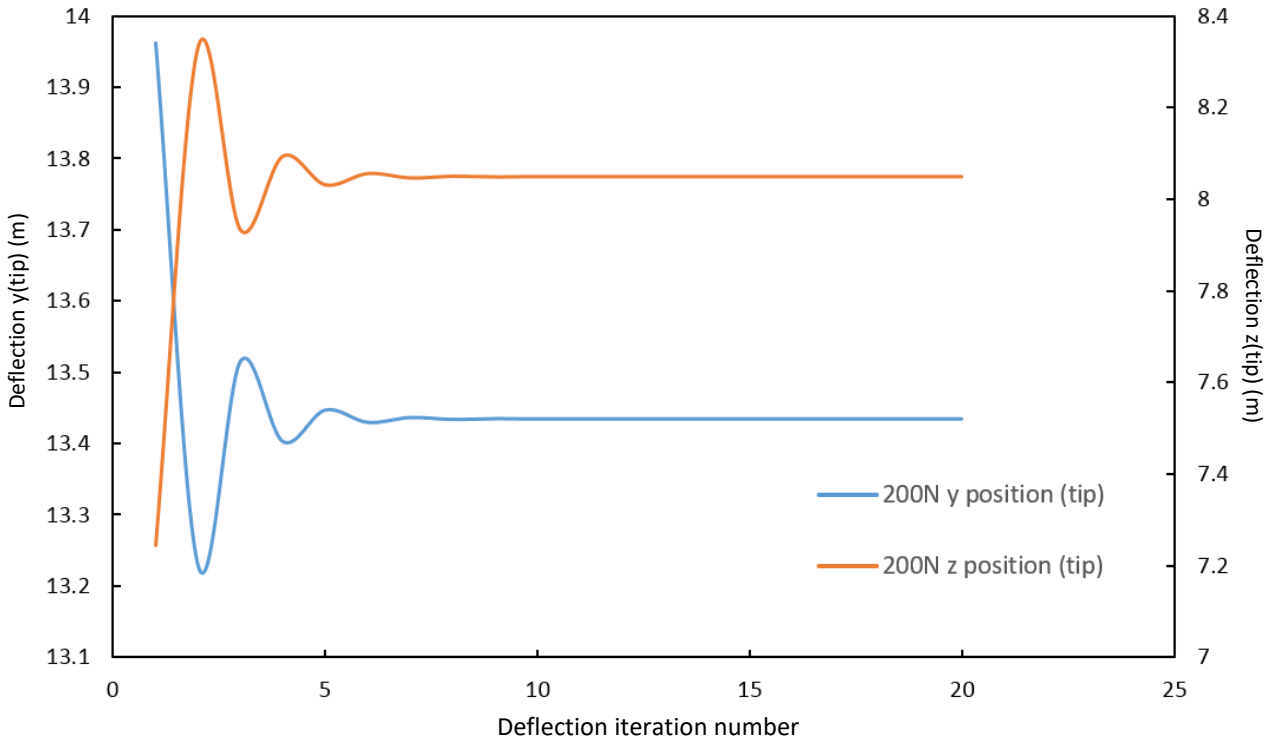

Fig 9.1. 200N Vertical Tip Load and 2 Bending Modes. Convergence of the y and z coordinate of the beam tip position, following 20 deflection iterations and using 30 number of terms in the Taylor approximation. As the number of deflection iterations increases, the z and y coordinate of the cantilever beam tip converge.

4.3.2 Bending Mode Variation

The final variable with major impact on the accuracy of the model, are the number of shapes, or bending modes used to construct the initial polynomial. The more bending modes, the more accurate the approximation of the deflection of the cantilever beam is. For the purpose of this analysis, only the first six bending modes have been considered. An increase in number of bending modes results in large quantities of complex mathematics that the computer takes time to process. The following figures show the variation in the (z,y) coordinate of the cantilever beam tip at 150N and 200N respectively using 20 iterations. For depiction purposes, the number of terms in the Taylor series for each polynomial is varied from 2 to 30. The polynomials for each bending mode are

$$\text{2BM:} \quad z(y,t) = q_1(t)\, y^2 + q_2(t)\, y^3 \tag{4.22}$$

$$\text{3BM:} \quad z(y,t) = q_1(t)\, y^2 + q_2(t)\, y^3 + q_3(t)\, y^4 \tag{4.23}$$

$$\text{4BM:} \quad z(y,t) = q_1(t)\, y^2 + q_2(t)\, y^3 + q_3(t)\, y^4 + q_4(t)\, y^5 \tag{4.24}$$

$$\text{5BM:} \quad z(y,t) = q_1(t)\, y^2 + q_2(t)\, y^3 + q_3(t)\, y^4 + q_4(t)\, y^5 + q_5(t)\, y^6. \tag{4.25}$$

$$\text{6BM:} \quad z(y,t) = q_1(t)\, y^2 + q_2(t)\, y^3 + q_3(t)\, y^4 + q_4(t)\, y^5 + q_5(t)\, y^6 + q_6(t)\, y^7 \tag{4.26}$$

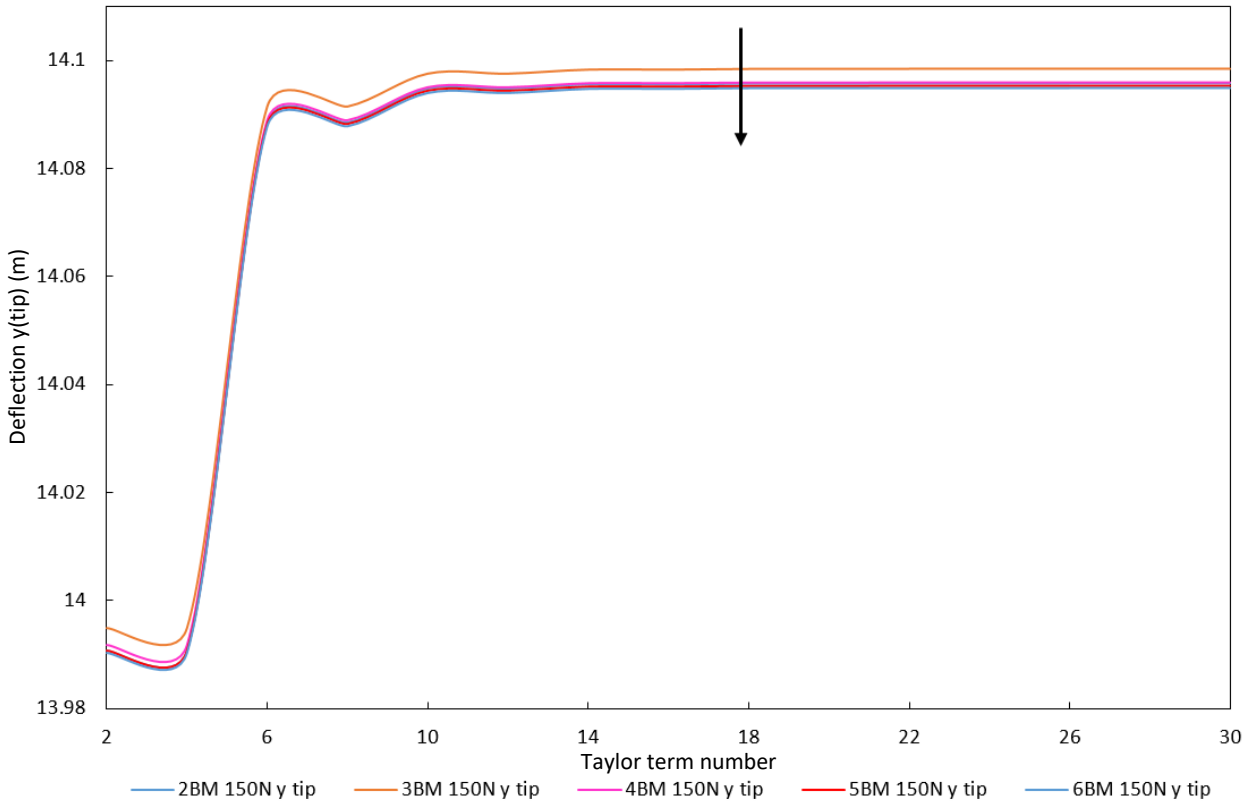

Fig 9.2. 150N Vertical Tip Load. Convergence of the y coordinate of the beam tip position for an increasing number of Taylor terms. The figure illustrates different coloured curves, depicting the effect of the increase of bending modes, ultimately leading to a convergence of the final deflection position of the tip of the beam.

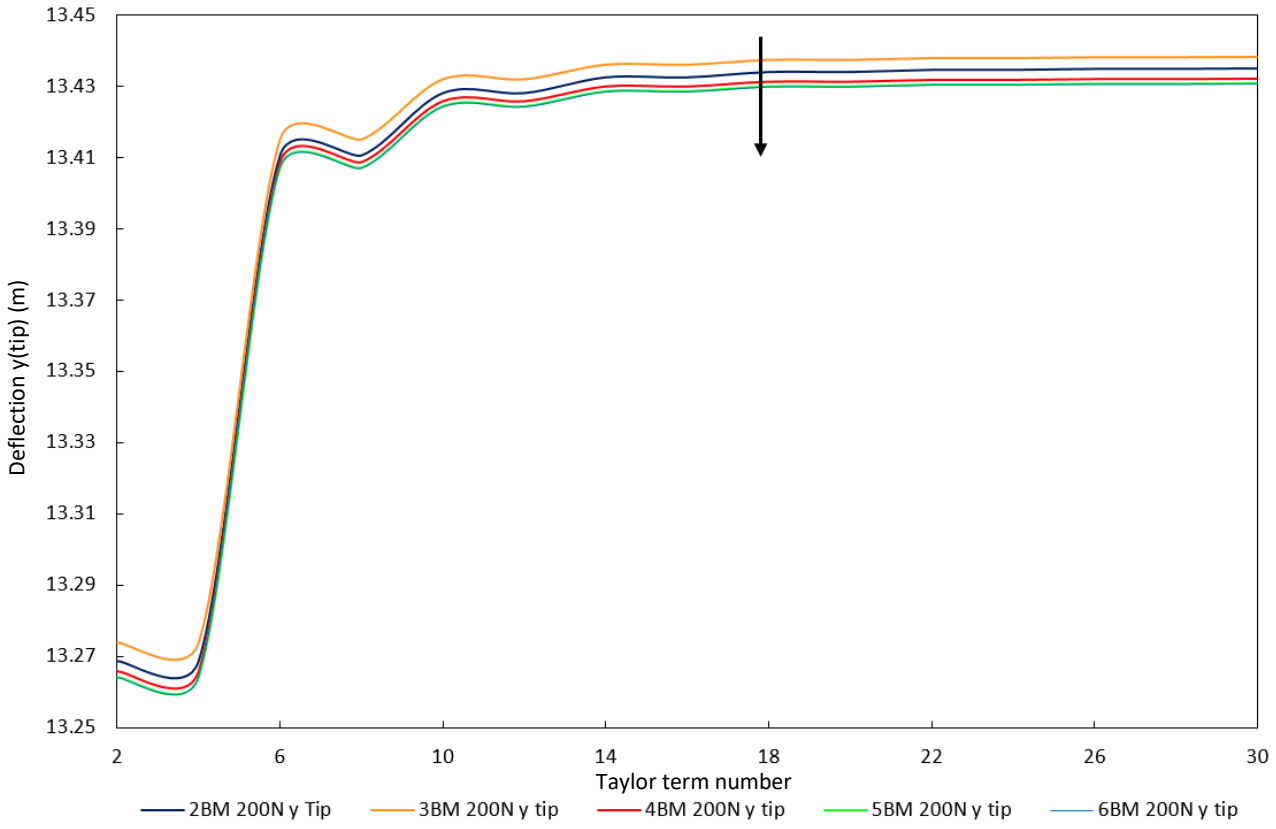

Fig 9.3. 200N Vertical Tip Load. Convergence of the y coordinate of the beam tip position for an increasing number of Taylor terms. The figure illustrates different coloured curves, depicting the effect of the increase of bending modes, ultimately leading to a convergence of the final deflection position of the tip of the beam.

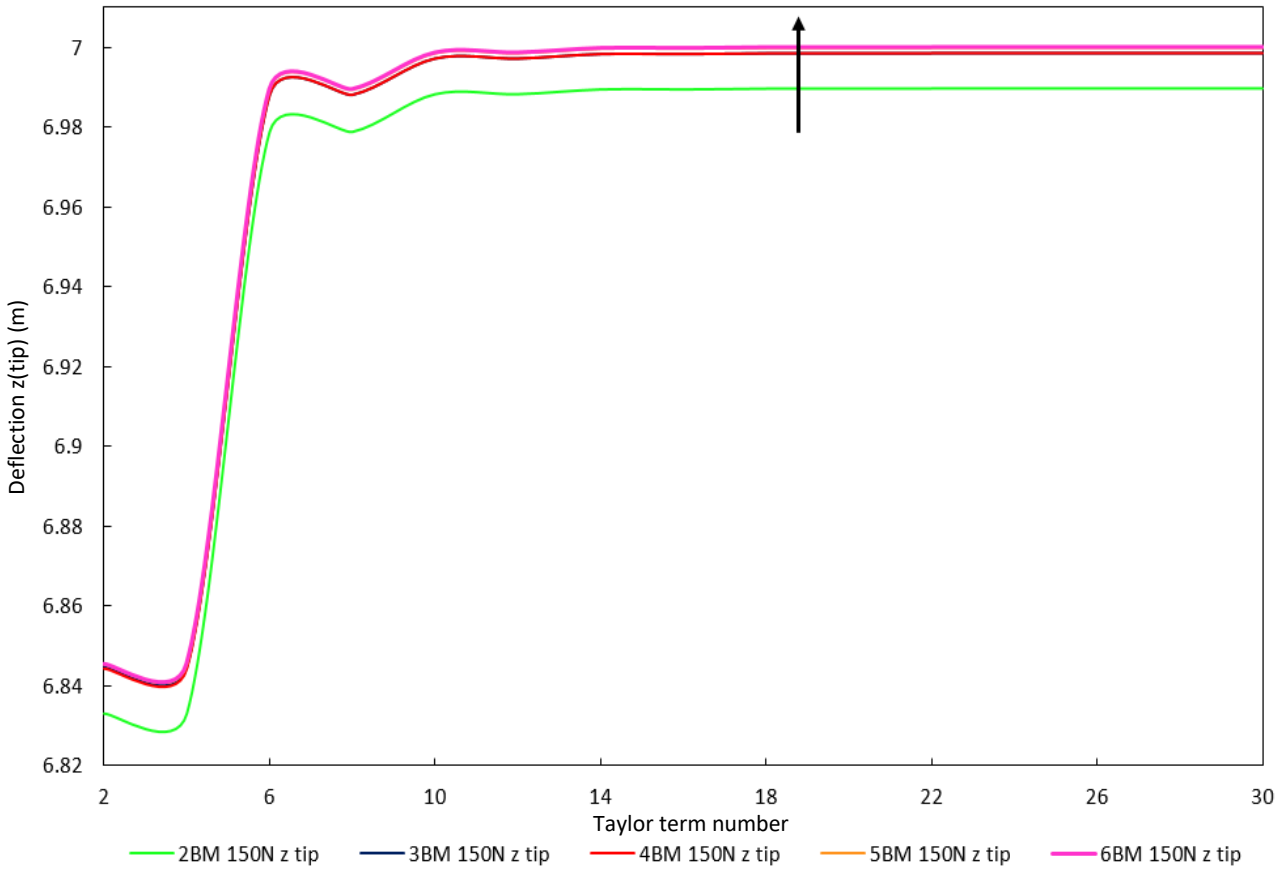

Fig 9.4. 150N Vertical Tip Load. Convergence of the z coordinate of the beam tip position for an increasing number of Taylor terms. The figure illustrates different coloured curves, depicting the effect of the increase of bending modes, ultimately leading to a convergence of the final deflection position of the tip of the beam.

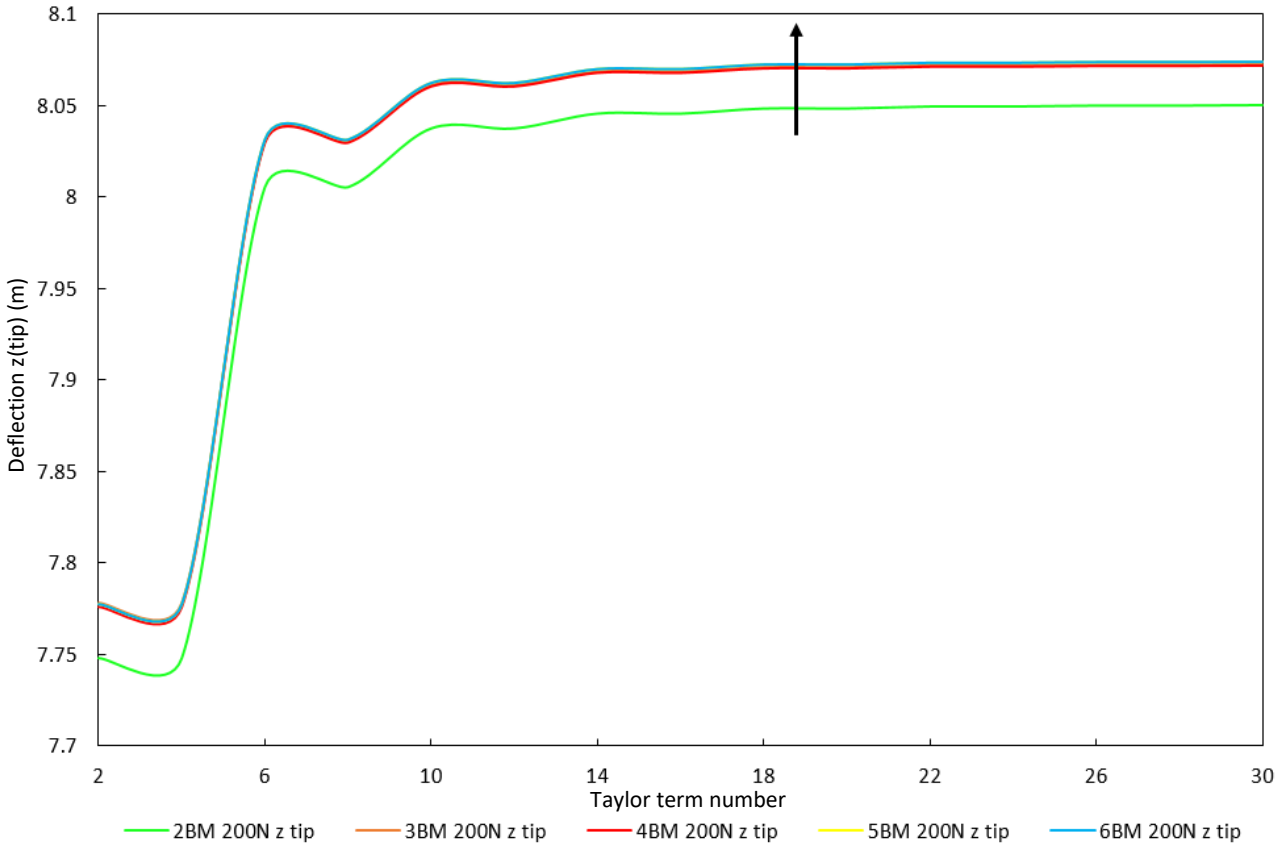

Fig 9.5. 200N Vertical Tip Load. Convergence of the z coordinate of the beam tip position for an increasing number of Taylor terms. The figure illustrates different coloured curves, depicting the effect of the increase of bending modes, ultimately leading to a convergence of the final deflection position of the tip of the beam.

4.3.3 HARW Large Deflection Bending Correction Method on Static Cantilever Beam – Application

To add meaning to the author's proposed research it is necessary to display the aforementioned methodology within a graph, in comparison to more simple, elementary beam theory and more complex literature findings.

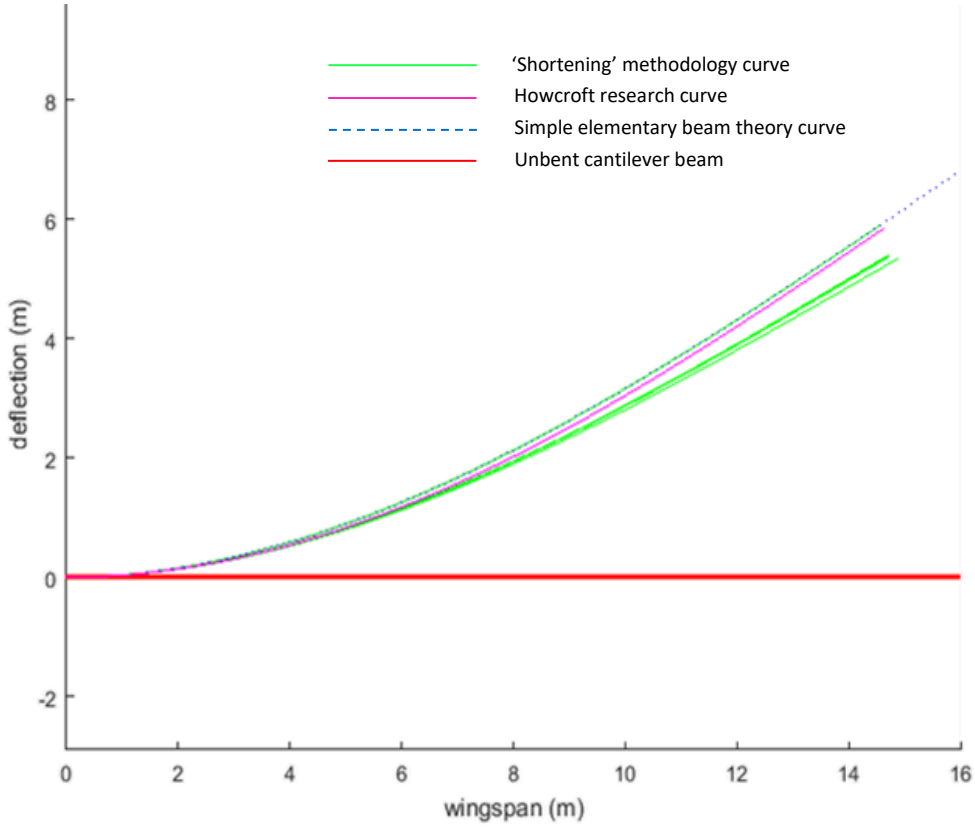

Fig 10. Figure showing three separate sets of results for the deflection of a cantilever beam of length 16m. The dotted blue curve depicts the simple elementary beam theory model for a cantilever beam, of flexural rigidity of 2E+4 Nm^2 and a 100N vertical tip force. The green curve depicts the curve with the aforementioned 'shortening' methodology. It can be see that the green curve converges onto one set curve shape. This curve has also been modelled for a cantilever beam subject to the same flexural rigidity and vertical tip load as the blue curve above. The third curve, depicted by a purple line, shows research data obtained by Christopher Howcroft from the University of Bristol. The red line on the graph shows the unbent cantilever beam of length 16m prior to large deflection.

Figure 10 shows the effectiveness of the author's research method against fundamental beam theory and current research by Howcroft (mid-publishing). It can be seen that the author's green curve accurately follows the general trend of the other two curves, although it does not reach the same vertical height. It must be noted that the length of the green curve (author's curve) has been calculated using the author's beam shortening method with a Taylor approximation series value of 30 and 10 iterations for convergence of the beam position.

Christopher Howcroft's curve modelling the large bending of a 16m cantilever beam with a 100N tip load was calculated using more complex mathematical methods. Christopher's method uses rotational states as opposed to conventional x,y,z states. This method of far greater complexity and therefore accuracy than considered in the author's methodology, is a good reference curve for studying the effect of a 100N vertical tip load on a cantilever beam. The 'actual' length of the bent cantilever beam can also be confirmed by looking at the author's estimated 'actual' length of the beam (end point of the green curve) and by looking at Christopher Howcroft's data and his calculated 'actual' length of the beam (end point of the purple curve). The length is similar and within 0.5% accuracy. This is a very successful result and its validity is strengthened through the difference in methods used to obtain the 'actual' length of the bent cantilever beam.

The apparent difference in vertical height can however, be criticised. The difference in vertical height is the case of an incorrect calculation of the second derivative of the displacement of the system.

As discussed in Chapter 3, the second derivative of the displacement of the system, or curvature, is used in the potential energy of the cantilever beam

$$U = \frac{1}{2}\int_0^L EI\left(\frac{\partial^2 z}{\partial y^2}\right)^2 dy. \tag{4.27}$$

This equation for the potential energy of the system is not strictly correct. Consider the shape of the deflected cantilever beam in figure 10 and let this shape be treated as a planar curve. The curvature of this curve, *K*, is defined as

$$K = \frac{d\vartheta}{dL} \tag{4.28}$$

where ϑ is the angle of a tangent at any point on the curve and *L* is the arc length of the curve. From calculus it is known that

$$tan\vartheta = \frac{dz}{dy} \tag{4.29}$$

and that

$$dy = (dy^2 + dz^2)^{\frac{1}{2}} = \left[1 + \left(\frac{dz}{dy}\right)^2\right]^{\frac{1}{2}} dy. \tag{4.30}$$

Differentiation gives the values of $d\vartheta$,

$$\frac{d\vartheta}{dt} = \frac{\frac{d^2 z}{dy^2}}{1 + \left(\frac{dz}{dy}\right)^2} \tag{4.31}$$

Substitution of these two equations into equation 4.28 yields the correct equation for the curvature of a curve, shown below [45].

$$K = \frac{\frac{d^2z}{dy^2}}{\left[1 + \left(\frac{dz}{dy}\right)^2\right]^{\frac{3}{2}}} = \left(\frac{\partial^2 z}{\partial y^2}\right) \tag{4.32}$$

The potential energy, can now be expressed as

$$U = \frac{1}{2}\int_0^L EI \left(\frac{\frac{d^2z}{dy^2}}{\left[1 + \left(\frac{dz}{dy}\right)^2\right]^{\frac{3}{2}}} \right)^2 dy \tag{4.33}$$

resulting in a modified potential energy term that would be used in modelling the deflection of the cantilever beam.

The difference in the expression for the curvature, or the second derivative of the curve, is thought to be one of the main factors responsible for the different in height and slight difference in shape of the curve.

Below are figures comparing the effect of an increase in the number of bending modes in the author's modelling of the deflection of a cantilever beam, in comparison to Christopher Howcroft's data. The number of terms in the Taylor approximation series has been kept at 30 throughout, and the number of iterations for convergence has been set to 20. The cantilever tip load has been increased to 150N, to show more pronounced 'shortening' effects. Flexural rigidity, EI, has remained at 2E+4 Nm^2.

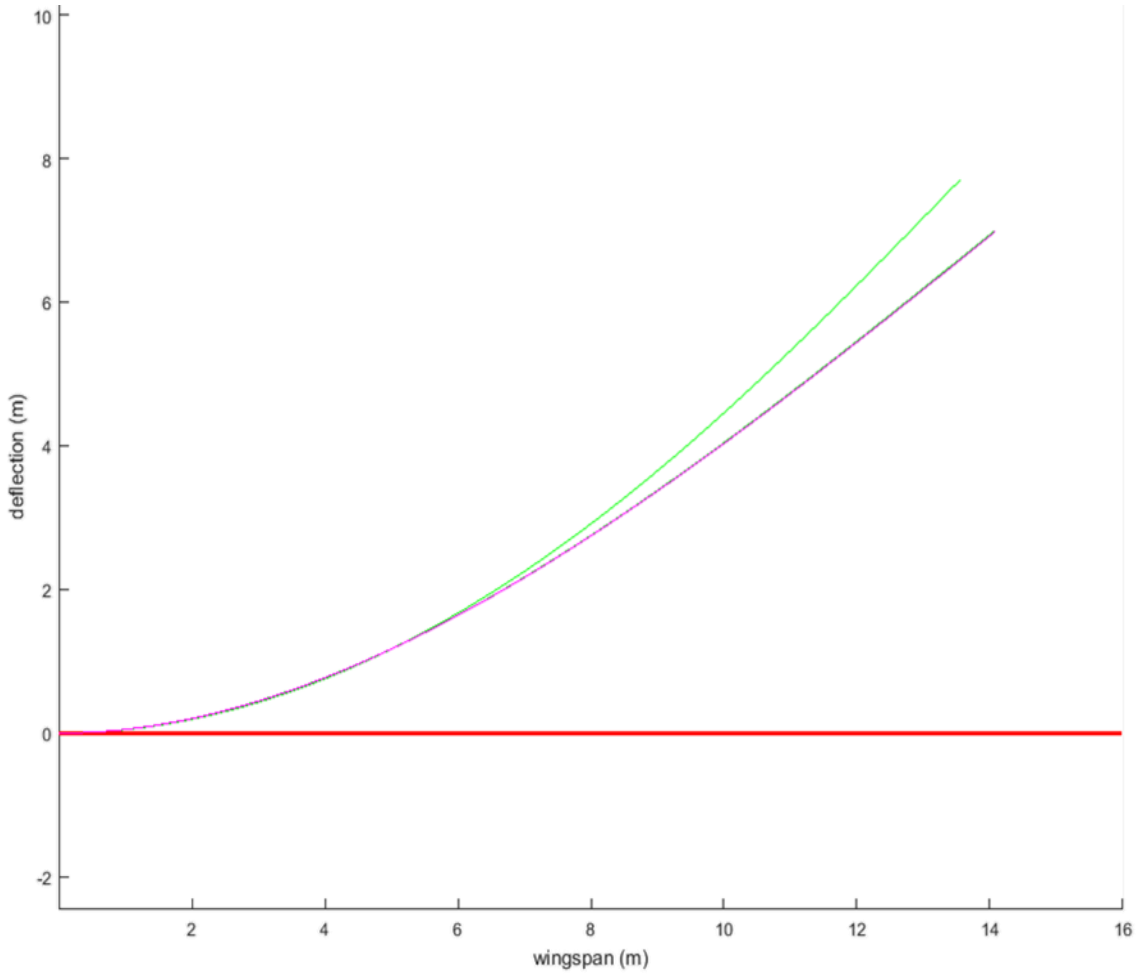

Fig 11. Graph showing Christopher Howcroft's deflection curve (green) for a 16m cantilever beam subject to a 150N vertical tip load, compared to two separate author's curves. One with three bending modes (blue), and one with six bending modes (purple). An undeflected 16m cantilever beam has been added for reference (red).

From figure 11, it is clear that there is no difference in increasing the number of bending modes of the system, on the physical appearance of the deflection of the cantilever beam. The blue and purple curves (three bending mode curve and six bending mode curve) overlap. It can be concluded that there is minimal change in this scenario.

CHAPTER 5

CONCLUSIONS

This thesis proposes a new method to improve existing flutter prediction models, flutter calculations and gust models for systems undergoing very large deflections. Although the author presents relatively fundamental research, its exploration places further emphasis and consideration on a topic that is often overlooked and not fully considered when looking at a highly flexible system undergoing large deflections. Whether this is the large deflection of structural cantilever beams in structural engineering, or the large deflection of highly flexible aircraft, the actual length of the beam must be established for accurate further modelling calculations. It can be concluded that a value for the position of the tip of a cantilever beam has successfully been calculated for the 'actual' length of a cantilever beam undergoing a large deflection, caused by a vertical point tip load. The shape of this cantilever beam deflection differs from that as suggested by elementary beam theory. The results obtained through the author's 'actual' length shortening calculator are coherent with literature results.

The occurrence of aeroelastic phenomena is inevitable in structures that have several bending modes and torsional modes. Although inevitable, prediction of these can prove extremely valuable to aircraft manufacturers, not only for safety-related issues, but for flight comfort in the suppression and alleviation of turbulence and gusts during flight. For high-aspect ratio wing aircraft, where non-linear effects dominate and limit design of aircraft, accurate prediction of flutter and other aeroelastic phenomena and prove structurally critical, especially when such highly flexible aircraft undergo extremely large deflections at very high altitude.

CHAPTER 6

FURTHER WORK

There a several changes that could be made to further this work and improve its method. Modifications and alterations could be made to the 'shortening' iterating code itself. The author considers the horizontal displacement and the apparent shortening of the beam in the y-axis, however, does not consider the potential shortening in the vertical, or z-axis. By inspection, this effect could take place in the vertical axis, which may also be the cause for the difference in cantilever tip height between Christopher Howcroft's curves and the author's curves.

Another major aspect that has not been is the altered curvature of the system, calculated in chapter 4.3.3. The inclusion of this modified second derivative in the equation for the potential energy of the cantilever beam undergoing a large deflection is imperative. However, the inclusion of this term and its evaluation could prove problematic. Due to its complexity, the evaluation of the term would result in a non-exact, numerical estimate using a range of numerical analysis methods. A method to overcome this issue would have to be establish in order to allow for the integration and solving for potential energy, work and ultimately the modified equations of motion of the bent cantilever beam.

Given the successful completion of these aforementioned steps, there is further work on high-aspect ratio wing (HARW) aircraft that was the author's original aim to be considered and evaluated. This includes:

One and Two Bending Modes

- the addition of a follower force to the concentrated tip load on the cantilever beam, in the form of a moment rotating anticlockwise at the tip of the cantilever beam
- the substitution of the concentrated tip load on the cantilever beam and follower force for a distributed load across the entire length of the cantilever beam
- the addition of a follower force to the distributed load on the cantilever beam, in the form of a moment rotating anticlockwise at the tip of the cantilever beam
- the modification of the system from static to dynamic, incorporating the kinetic energy for use in the Lagrange analysis
- the conversion of the cantilever beam from a two-dimensional (2-D) cantilever beam to a three-dimensional (3-D), rectangular cantilever plate
- the division of the 3-D rectangular cantilever plate into set equidistant strips and hence the incorporation of aerodynamic strip theory, modelling the plate as a simple aerodynamic aerofoil
- the modification of the shape of the rectangular cantilever plate into the same of a typical aircraft wing
- the addition of the lift force distribution according to a specific NACA 4 digit aerofoil

- the amalgamation of all these modifications in the calculation and determination of flutter velocity, use of the ‘p-k’ method (frequency matching) and establishing V-g plots.

One and Two Bending Modes + One and Two Torsion Modes

- the repetition of the above steps, however with the introduction of torsional degrees of freedom in the three-dimensional x-z axis
- the addition of more complex wing geometry
- the addition of control surfaces and further modification in lift distribution
- the analysis of the occurrence of flutter on these control surfaces
- the inclusion of aerodynamic and structural damping
- the analysis of the change in position of the mass and elastic axes
- the introduction of further bending and torsional modes and analysis of their coupling effects
- the inclusion of a second wing, rear wings, amalgamation and therefore the consideration of the whole aircraft; including rigid body modes and effect of loads
- Limit cycle oscillations (LCO) determination and further analysis
- Introduction of gusts and effect of turbulence on the system.

There are many more aspects that could have been explored and investigated for a high-aspect ratio wing aircraft, perhaps, more suitable for a higher doctoral degree, of longer duration.

REFERENCES

[1] Kehoe M. NASA Technical Memorandum 4720, A Historical Overview of Flight Flutter Testing. 1995.

[2] Garrick I, Reed III W. Historical Development of Aircraft Flutter. Journal of Aircraft. 1981;18(11):897-912.

[3] 1905-1915 Wright Bent-End Propellers [Internet]. Wright-brothers.org. 2018 [cited 05 October 2017]. Available from: http://www.wright-brothers.org/Information_Desk/Just_the_Facts/Engines_&_Props/1905-1915_Props.htm

[4] Hill G. Advances in Aircraft Structural Design. Third Anglo-American Aeronautical Conference. Royal Aeronautical Society; 1951.

[5] Brewer G. The Collapse of Monoplane Wings. Flight. 1913;5:33.

[6] Bairstow L, Fage A. Oscillations of the Tail Plane and Body of an Aeroplane. Aeronautical Research Committee R&M; 1916.

[7] Blasius H. Uber Schwingungserscheinungen an Einholmigen Unterflugeln. Z Flugtech u Motorluftschif. 1925;16:39-42.

[8] Fung Y. An introduction to the theory of aeroelasticity. New York: Dover Publications; 1993.

[9] Birnbaum W. Das ebene Problem des schlagenden Flügels. ZAMM - Zeitschrift für Angewandte Mathematik und Mechanik. 1924;4(4):277-292.

[10] Wagner H. Über die Entstehung des dynamischen Auftriebes von Tragflügeln. ZAMM - Zeitschrift für Angewandte Mathematik und Mechanik. 1925;5(1):17-35.

[11] Glauert H. The Force and Moment on an Oscillating Aerofoil. H.M. Stationery Office; 1929.

[12] Küssner H. Schwingungen von Flugzeugflügeln. Luftfahrt-Forsch. 1929;4(2):41-62.

[13] Theodorsen T. Report No. 496, General theory of aerodynamic instability and the mechanism of flutter. National Advisory Committee for Aeronautics Langley Aeronautical Lab. 1949.

[14] Garrick I. An Appreciation of the Contributions of Theodore Theodorsen. Proceedings of the Theodorsen Colloqium, Det Kongelige Norske Videnskabers Selskab. 1976.

[15] Smilg B, Wasserman L. Application of three-dimensional flutter theory to aircraft structures. Dayton, Ohio: War Dept., Air Corps Material Div.; 1942.

[16] Tipler P, Mosca G. Physics for scientists and engineers. New York: W.H. Freeman; 2004.

[17] Walker J, Halliday D, Resnick R. Fundamentals of physics. Hoboken, NJ: Wiley; 2008.

[18] Billah K, Scanlan R. Resonance, Tacoma Narrows bridge failure, and undergraduate physics textbooks. American Journal of Physics. 1991;59(2):118-124.

[19] Zhao Y. Flutter suppression of a high aspect-ratio wing with multiple control surfaces. Journal of Sound and Vibration. 2009;324(3-5):490-513.

[20] Borglund D, Kuttenkeuler J. Active Wing Flutter Suppression using a trailing edge flap. Journal of Fluids and Structures. 2002;16(3):271-294.

[21] Andrighettoni M, Mantegazza P. Multi-Input/Multi-Output Adaptive Active Flutter Suppression for a Wing Model. Journal of Aircraft. 1998;35(3):462-469.

[22] Liu Y, Xie C, Yang C, Cheng J. Gust response analysis and wind tunnel test for a high-aspect ratio wing. Chinese Journal of Aeronautics. 2016;29(1):91-103.

[23] Dong G, Xu M, Chen S. Nonlinear Gust Response Analysis of Free Flexible Aircraft. International Journal of Intelligent Systems and Applications. 2013;5(2):1-15.

[24] Su W, S. Cesnik C. Dynamic Response of Highly Flexible Flying Wings. AIAA Journal. 2011;49(2):324-339.

[25] Tari H, Kinzel G, Mendelsohn D. Cartesian and piecewise parametric large deflection solutions of tip point loaded Euler–Bernoulli cantilever beams. International Journal of Mechanical Sciences. 2015;100:216-225.

[26] Bennig G. Atomic force microscope and method for imaging surfaces with atomic resolution. US; 4724318, 1988.

[27] Leo D. Engineering Analysis of Smart Material Systems. New Jersey: John Wiley & Sons; 2007.

[28] Bisshopp K, Drucker D. Large Deflection of Cantilever Beams. Q Appl Math. 1945;3(3):272-275.

[29] Gross S, Lehr E. Die federn, ihre gestaltung und berechnung. 1938.

[30] Barten H. On the deflection of a cantilever beam. Quarterly of Applied Mathematics. 1944;2(2):168-171.

[31] Jahnke E, Emde F. Funktionentafeln Mit Formeln Und Kurven. Dover Publications; 1943.

[32] Dado M, Al-Sadder S. A new technique for large deflection analysis of non-prismatic cantilever beams. Mechanics Research Communications. 2005;32(6):692-703.

[33] Beléndez T, Neipp C, Beléndez A. Large and small deflections of a cantilever beam. European Journal of Physics. 2002;23(3):371-379.

[34] Freeman J. Mathematical theory of deflection of beam. Phil Mag. 1946;(35):551.

[35] Wang C, Watson L. On the large deformations of C-shaped springs. International Journal of Mechanical Sciences. 1980;22(7):395-400.

[36] Mau S. Elastica Solution of Braced Struts. Journal of Engineering Mechanics. 1990;116(3):688-697.

[37] Lee B, Oh S. Elastica and buckling load of simple tapered columns with constant volume. International Journal of Solids and Structures. 2000;37(18):2507-2518.

[38] Chen L. An integral approach for large deflection cantilever beams. International Journal of Non-Linear Mechanics. 2010;45(3):301-305.

[39] Ang M, Wang Wei, Low Teck-Seng. On the estimation of the large deflection of a cantilever beam. Proceedings of IECON '93 - 19th Annual Conference of IEEE Industrial Electronics. 1993.

[40] Golley B. The finite element solution of a class of elastica problems. Computer Methods in Applied Mechanics and Engineering. 1984;46(2):159-168.

[41] Schmidt W. Nonlinear bending of beams using the finite element method. Computers & Structures. 1978;8(1):153-158.

[42] Kooi B. A unilateral contact problem with the heavy elastica solved by use of finite elements. Computers & Structures. 1985;21(1-2):95-103.

[43] Kooi B, Kuipers M. A unilateral contact problem with the heavy elastica. International Journal of Non-Linear Mechanics. 1984;19(4):309-321.

[44] Saje M, Srpčič S. Large deformations of in-plane beam. International Journal of Solids and Structures. 1985;21(12):1181-1195.

[45] Kopmaz O, Gündoğdu Ö. On the Curvature of an Euler–Bernoulli Beam. International Journal of Mechanical Engineering Education. 2003;31(2):132-142.

[46] Howcroft C, Calderon D, Lambert L, Castellani M, Cooper J, Lowenberg M et al. Aeroelastic Modelling of Highly Flexible Wings. 15th Dynamics Specialists Conference. 2016.

[47] Patil M, Hodges D, S. Cesnik C. Nonlinear Aeroelasticity and Flight Dynamics of High-Altitude Long-Endurance Aircraft. Journal of Aircraft. 2001;38(1):88-94.

[48] [Internet]. 2009 [cited 10 October 2017]. Available from: https://upload.wikimedia.org/wikipedia/commons/8/84/ASH_31_Mi_Flug_001_20090421.JPG

[49] Airbus Zephyr [Internet]. 2016 [cited 10 October 2017]. Available from: http://defence.airbus.com/wp-content/uploads/2016/05/zephyr_intro.jpg

[50] Tang D, Dowell E. Experimental and Theoretical Study on Aeroelastic Response of High-Aspect-Ratio Wings. AIAA Journal. 2001;39(8):1430-1441.

[51] Dowell E, Traybar J, Hodges D. An experimental-theoretical correlation study of non-linear bending and torsion deformations of a cantilever beam. Journal of Sound and Vibration. 1977;50(4):533-544.

[52] Spada C, Afonso F, Lau F, Suleman A. Nonlinear aeroelastic scaling of high aspect-ratio wings. Aerospace Science and Technology. 2017;63:363-371.

[53] Mashayekhi M, Sedaghat A, Ghayour M. Linear Flutter Prediction for a Cantilever Wing Model. 14th Annual Mechanical Engineering Conference. 2006.

[54] Wright J, Cooper J. Introduction to Aircraft Aeroelasticity and Loads, 2nd Edition. John Wiley & Sons; 2015.

[55] Han J, Tani J, Qiu J. Active flutter suppression of a lifting surface using piezoelectric actuation and modern control theory. Journal of Sound and Vibration. 2006;291(3-5):706-722.

[56] Abbott I, VonDoenhoff A. Theory of wing sections. New York, N.Y.: Dover Publ.; 1959.

[57] Ovesy H, Nikou A, Shahverdi H. Flutter analysis of high-aspect-ratio wings based on a third-order nonlinear beam model. Proceedings of the Institution of Mechanical Engineers, Part G: Journal of Aerospace Engineering. 2012;227(7):1090-1100.

[58] Otto P. A proof of arc length [Internet]. 2011 [cited 10 September 2017]. Available from: http://mason.gmu.edu/~potto/doc/calculationOfArcLength.pdf

[59] Jowkowski N. On annexed vortices. Proc of Physical Section of the Natural Science Society. 1906;13(2):12-25 (in Russian).